



**VICTORIA UNIVERSITY**  
MELBOURNE AUSTRALIA

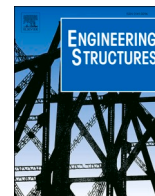
*Higher-order trigonometric series-based analytical solution to free transverse vibration of suspended laminated composite slabs*

This is the Published version of the following publication

Gohari, Soheil, Ahmed, Mizan, Liang, Qing, Molla, Tesfaye, Kajtaz, Mladenko, Tse, Kwong Ming and Burvill, Colin (2023) Higher-order trigonometric series-based analytical solution to free transverse vibration of suspended laminated composite slabs. *Engineering Structures*, 296 (20). ISSN 0141-0296

The publisher's official version can be found at  
<https://www.sciencedirect.com/science/article/pii/S0141029623013172?via%3Dihub>  
Note that access to this version may require subscription.

Downloaded from VU Research Repository <https://vuir.vu.edu.au/47390/>



# Higher-order trigonometric series-based analytical solution to free transverse vibration of suspended laminated composite slabs

Soheil Gohari<sup>a</sup>, Mizan Ahmed<sup>b</sup>, Qing Quan Liang<sup>c,\*</sup>, Tesfaye Molla<sup>a</sup>, Mladenko Kajtaz<sup>d</sup>, Kwong Ming Tse<sup>e</sup>, Colin Burvill<sup>a</sup>

<sup>a</sup> Department of Mechanical Engineering, The University of Melbourne, Parkville, VIC 3010, Australia

<sup>b</sup> Centre for Infrastructure Monitoring and Protection, School of Civil and Mechanical Engineering, Curtin University, Kent Street, Bentley, WA 6102, Australia

<sup>c</sup> College of Sport, Health, and Engineering, Victoria University, PO Box 14428, Melbourne, VIC 8001, Australia

<sup>d</sup> School of Engineering, RMIT University, PO Box 71, Bundoora, VIC 3083, Australia

<sup>e</sup> Department of Mechanical and Product Design Engineering, School of Engineering, Swinburne University of Technology, Australia

## ARTICLE INFO

### Keywords:

Analytical solution  
Elasticity theory  
Higher-order trigonometric series  
Free transverse vibration  
Suspended laminated composite slabs

## ABSTRACT

Suspended floors can be designed as effective pendulum seismic isolators for high-rise buildings. However, research studies on the free vibration of suspended laminated composite slabs are relatively limited. This paper presents a comprehensive analytical solution to the free vibration problem of suspended laminated composite slabs. The equations of elasticity are used to establish the equation of motion. The critical factors influencing free vibration are explicitly considered, including the material anisotropy, number of layers, elastic properties, rotatory inertia, and transverse shear of plates. The higher-order trigonometric series are utilized to solve the dynamic equations. The developed analytical solution is a complete and realistic form of the existing analytical solutions in literature and has the capability of converging fast. The proposed analytical solution does not have a dependency on the shape function as well as separate-of-variable forms unlike the Finite Element Method (FEM). Moreover, the FEM requires an in-depth mesh convergence analysis, particularly for higher-magnitude natural frequencies, which is not the case for the proposed analytical solution for any infinite range of eigenfrequencies. The proposed solution procedure is first verified by the simplified problems available in the literature. For more complex problems, the finite element analysis results obtained from Abaqus are employed to validate the analytical solution. The comparison demonstrates that the proposed analytical solution is accurate and reliable for a wide range of case-study examples. It is found that the natural frequencies of suspended laminated composite slabs are significantly influenced by the crucial factors under investigation.

## 1. Introduction

Laminated composite plates have been widely used in aerospace, automobile, civil, and marine engineering due to their high strength-to-weight and strength-to-stiffness ratios [1,2]. The design of engineering structures with various geometries and shapes for dynamic instability has been demonstrated to be a significant challenge. Therefore, dynamic systems incorporating laminated composite plates must be properly studied to develop effective seismic isolation techniques for such systems [3,4].

One of the main applications of plates is in plated building structures such as floors and ceilings made of plate slabs [5,6]. An innovative

concept of seismic isolation has been proposed by researchers [7–9], which utilizes the suspended floor and ceiling slab system as a seismic isolator for buildings as illustrated in Fig. 1. This system has shown to provide effective vibration isolation of a building in regions where the seismic activities are high [7]. The advantages of this concept are that the structural vibration can be isolated or the damage can be concentrated on the replaceable or repairable elements and the residual drift is effectively contained. There are several studies in this area with promising results [10–13].

Mahmoud and Chulawat [14] emphasized on the importance of the dynamic response analysis of suspended slab systems under dynamic excitation. In their study, the suspended slabs were used as pendulum

\* Corresponding author at: College of Sport, Health, and Engineering, Victoria University, PO Box 14428, Melbourne, VIC 8001, Australia.

E-mail addresses: [soheil.gohari@unimelb.edu.au](mailto:soheil.gohari@unimelb.edu.au) (S. Gohari), [mizan.ahmed@curtin.edu.au](mailto:mizan.ahmed@curtin.edu.au) (M. Ahmed), [Qing.Liang@vu.edu.au](mailto:Qing.Liang@vu.edu.au) (Q.Q. Liang), [tesfaye.molla@unimelb.edu.au](mailto:tesfaye.molla@unimelb.edu.au) (T. Molla), [mladenko.kajtaz@rmit.edu.au](mailto:mladenko.kajtaz@rmit.edu.au) (M. Kajtaz), [ktse@swin.edu.au](mailto:ktse@swin.edu.au) (K.M. Tse), [colb@unimelb.edu.au](mailto:colb@unimelb.edu.au) (C. Burvill).

<https://doi.org/10.1016/j.engstruct.2023.116902>

Received 3 June 2023; Received in revised form 26 August 2023; Accepted 14 September 2023

Available online 25 September 2023

0141-0296/© 2023 The Author(s). Published by Elsevier Ltd. This is an open access article under the CC BY license (<http://creativecommons.org/licenses/by/4.0/>).

Tuned Mass Damper (TMD) in order to decrease the response of steel frames under an excitation caused by earthquake. It was concluded that the suspended floor systems can be used in tall buildings to decrease the dynamic response of the main frames and to isolate particular floors. However, several important factors were not taken into account in their investigation, such as the calculation of the natural frequency of each suspended floor system, proper selection of material properties to effectively reduce the free vibration response, and the selection of appropriate thickness and geometry for such purpose. It is widely accepted that taller buildings have lower natural frequencies. Consequently, high-frequency earthquake waves would damage small buildings and low-frequency waves would damage taller buildings. Therefore, the proper selection of material properties, geometry, thickness, and size can greatly reduce the resonance phenomena during seismic activities.

The first ever investigation into the vibration of plates with various sizes under different boundary condition was done by NASA [15]. They used the simplified Fourier series as a general solution to the classical equations of motion in space and verified the results by the experiments. Although they considered the anisotropy effect as well as boundaries on the eigenfrequencies of suspended plate slabs, the influence of rotatory inertia and transfer shear of the plates was not studied. Li et al. [16] developed a theoretical framework using an up-to-date Hamiltonian system-based simplistic superposition method, which is useful when the solution procedure in the simplistic space is sought. The in-plane eigenfrequencies of the suspended thin isotropic plates and their corresponding mode shapes were obtained using their analytical method. However, the effects of both shear deformation and rotary inertia of the plates and material anisotropy on the free vibration response were disregarded. Zhong et al. [17] proposed an analytical solution that used the finite cosine integral transform method to calculate the eigenfrequencies of the suspended thin isotropic plates resting on an elastic foundation. Their analytical solution procedure ignored the influence of material anisotropy, transverse shear deformation, and rotatory inertia of the plates, making it applicable to very limited cases. Hu et al. [18] extended the work done by Li et al. [16] by developing a more complete Hamiltonian system-based simplistic superposition method for in-plane free vibration of thin plates considering material anisotropy. Despite the novelty of such solution, it still lacks the consideration of the rotary inertia and transverse shear of the plates. Dozio [19] developed an accurate upper-bound analytical solution to the free in-plane vibration problem of laminated composite plates with symmetrical stacking sequence and various boundary conditions. The Partial Differential Equations (PDEs) of motion were solved by using the Ritz method. Their

study excluded the influence of rotatory inertia and transfer shear of the plates. Wang et al. [20] developed a closed-form theoretical framework to explore the free in-plane vibration of rectangular isotropic plates under diverse range of boundary conditions. Their solution is applicable to suspended plates. However, their study has several limitations, such as ignoring the transfer shear deformation and rotatory inertia and material anisotropy. Furthermore, their exact solution containing the separate-of-variable form cannot accurately capture the modes of diagonal symmetry in suspended plates. Du et al. [21] presented an improved Fourier series coupled with four additional supplementary functions for predicting the free vibration response of plates under various boundary conditions including suspended plates. Such analytical solution cannot, however, be used for thick or moderately thick plates as the effect of transverse shear deformation is ignored. Furthermore, the accuracy of the results decreases significantly with increasing the order of the frequency mode due to ignoring the influence of rotatory inertia. Finally, their solution is only applicable to isotropic materials. Bardell et al. [22] proposed an analytical solution based on the Rayleigh-Ritz method to calculate the free in-plane vibration of rectangular plates. Their solution procedure is applicable to suspended plate slabs. However, like many studies discussed above, their solution can only be used for very limited cases because the effects of material anisotropy, rotatory inertia, and transverse shear deformation are not considered.

Upon in-depth review of the literature, it is revealed that there is no complete analytical solution that accounts for the crucial factors influencing the free vibration response of suspended plate slabs. Therefore, these shortcomings have motivated us to develop a comprehensive analytical solution procedure encompassing the effect of rotatory inertia, transverse shear, material anisotropy, and optimum laminate stacking sequence all together. The proposed analytical solution is based on the higher-order trigonometric series and 3D elasticity principles without a need to predetermine any shape function or separate-of-variable form. As a result, the formulated solution warrants the accuracy of the obtained eigenfrequencies. The proposed analytical solution leads to fast convergence, thereby significantly reducing the computational time. Moreover, it is independent of any modification of the theoretical formulation and the simulation codes during the parametric studies unlike the Finite Element Method (FEM) [23]. Furthermore, it can be a reliable benchmark for large eigenfrequencies analysis since the mesh refinement is not required unlike numerical methods such as FEM [23].

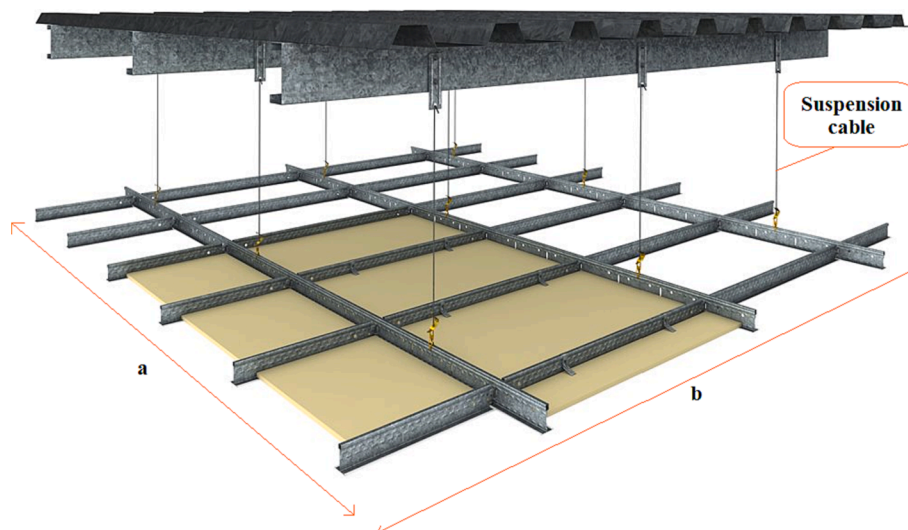


Fig. 1. An example of a suspended plate slab made of multiple materials [9].

**2. Mathematical formulation**

The lateral free vibration response of a thick composite plate slab including the influence of transverse shear and rotatory inertia, which is based on the three dimensional (3D) elasticity equations, can be obtained using Eqs. (1)–(3) [24]:

$$K_s A_{55} \left( \frac{\partial \phi_x(x, y, t)}{\partial x} + \frac{\partial^2 W(x, y, t)}{\partial x^2} \right) + K_s A_{44} \left( \frac{\partial \phi_y(x, y, t)}{\partial y} + \frac{\partial^2 W(x, y, t)}{\partial y^2} \right) - \rho_1 \left( \frac{\partial^2 W(x, y, t)}{\partial t^2} \right) = 0 \tag{1}$$

$$D_{11} \frac{\partial^2 \phi_x(x, y, t)}{\partial x^2} + D_{66} \frac{\partial^2 \phi_x(x, y, t)}{\partial y^2} + (D_{12} + D_{66}) \frac{\partial^2 \phi_y(x, y, t)}{\partial x \partial y} - K_s A_{55} \left( \phi_x(x, y, t) + \frac{\partial W(x, y, t)}{\partial x} \right) - \rho_2 \left( \frac{\partial^2 \phi_x(x, y, t)}{\partial t^2} \right) = 0 \tag{2}$$

$$(D_{12} + D_{66}) \frac{\partial^2 \phi_x(x, y, t)}{\partial x \partial y} + D_{66} \frac{\partial^2 \phi_y(x, y, t)}{\partial x^2} + D_{22} \frac{\partial^2 \phi_y(x, y, t)}{\partial y^2} - K_s A_{44} \left( \phi_y(x, y, t) + \frac{\partial W(x, y, t)}{\partial y} \right) - \rho_2 \left( \frac{\partial^2 \phi_y(x, y, t)}{\partial t^2} \right) = 0 \tag{3}$$

where,

$$W(x, y, t) = W(x, y) \sin(\omega_j t + \omega_0) = \left[ \frac{1}{ab} w(0, 0) + \frac{2}{ab} \sum_{n=1}^{\infty} w(0, n) \cos(\beta_n y) + \frac{2}{ab} \sum_{m=1}^{\infty} w(m, 0) \cos(\alpha_m x) + \frac{4}{ab} \sum_{m=1}^{\infty} \sum_{n=1}^{\infty} w(m, n) \cos(\alpha_m x) \cos(\beta_n y) \right] \sin(\omega_j t + \omega_0) \tag{4}$$

$$\phi_x(x, y, t) = \phi_x(x, y) \sin(\omega_j t + \omega_0) = \left[ \frac{2}{ab} \sum_{m=1}^{\infty} \bar{\phi}_x(m, 0) \sin(\alpha_m x) + \frac{4}{ab} \sum_{m=1}^{\infty} \sum_{n=1}^{\infty} \bar{\phi}_x(m, n) \sin(\alpha_m x) \cos(\beta_n y) \right] \times \sin(\omega_j t + \omega_0) \tag{5}$$

$$\phi_y(x, y, t) = \phi_y(x, y) \sin(\omega_j t + \omega_0) = \left[ \frac{2}{ab} \sum_{n=1}^{\infty} \bar{\phi}_y(0, n) \sin(\beta_n y) + \frac{4}{ab} \sum_{m=1}^{\infty} \sum_{n=1}^{\infty} \bar{\phi}_y(m, n) \cos(\alpha_m x) \sin(\beta_n y) \right] \times \sin(\omega_j t + \omega_0) \tag{6}$$

$$\rho_1 = \rho H \tag{7}$$

$$\rho_2 = \left( \frac{\rho}{3} \right) H^3 \tag{8}$$

where, the length and width of the plate are  $a$  and  $b$ , respectively [25];  $x$ ,

$y$ , and  $z$  are the elements of the Cartesian coordinate system and  $t$  is time;  $\rho$  and  $H$  are the density and total thickness of a composite plate, respectively [25];  $\rho_1$  and  $\rho_2$  stand for the first and second densities of a rectangular plate, respectively, which are associated with the rotatory inertia of a plate;  $W$  is the vertical dynamic response associated with the flexural deformation which can be obtained using Eq.4;  $\phi_x$  and  $\phi_y$  are the transverse shear rotation effects, which depend on the position and time, respectively [26];  $K_s$  represents the transverse shear correction factor in a thick plate which is equal to 5/6 [27];  $D_{11}$ ,  $D_{22}$ ,  $D_{12}$ , and  $D_{66}$  represent the flexural rigidity of an orthotropic material [28,29];  $A_{44}$  and  $A_{55}$  are the transverse shear stiffness of an orthotropic material in the  $yz$  and  $xz$  planes, respectively [30];  $\omega_j$  and  $\omega_0$  stand for the  $j$ th natural frequency of free vibration and initial frequency, respectively [31]. In Eqs.4–6,  $W(x, y)$ ,  $\phi_x(x, y)$ , and  $\phi_y(x, y)$  stand for the mode shapes of a thick composite plate under free transverse vibration excitation. The mode shapes of vibrations are independent of time.

When considering a suspended plate slab, it is assumed that all edges are free and any point/element within these edges possesses six degrees of freedom. As a result, all edges can freely rotate along any axis ( $M_x = M_y = M_z = 0$ ) and move in any direction ( $U_x = U_y = U_z = 0$ ), in which  $M_x$ ,  $M_y$ , and  $M_z$  are the bending moments and  $U_x$ ,  $U_y$ , and  $U_z$  are the displacements along the  $x$ ,  $y$ , and  $z$  directions, respectively.

The higher-order finite integral transforms of the shape functions in Eqs. (4)–(6) are derived for a suspended thick composite slab as stated by Eqs. (9)–(11), respectively:

$$w(m, n) = \int_0^a \int_0^b W(x, y) \cos(\alpha_m x) \cos(\beta_n y) dx dy \tag{9}$$

$$\bar{\phi}_x(m, n) = \int_0^a \int_0^b \phi_x(x, y) \sin(\alpha_m x) \cos(\beta_n y) dx dy \tag{10}$$

$$\bar{\phi}_y(m, n) = \int_0^a \int_0^b \phi_y(x, y) \cos(\alpha_m x) \sin(\beta_n y) dx dy \tag{11}$$

In the next step, assuming that the initial frequency is equal to zero, Eqs. (4)–(6) are first substituted into Eqs. (1)–(3) and the higher-order finite integral transforms are then taken over Eqs. (1)–(3), resulting in Eqs. (12)–(14), respectively:

$$\begin{aligned}
& K_s A_{55} \int_0^a \int_0^b \frac{\partial \phi_x(x, y)}{\partial x} \sin(\omega_j t) \cos(\alpha_m x) \cos(\beta_n y) dx dy + K_s A_{55} \int_0^a \int_0^b \frac{\partial^2 W(x, y)}{\partial x^2} \sin(\omega_j t) \cos(\alpha_m x) \cos(\beta_n y) dx dy \\
& + K_s A_{44} \int_0^a \int_0^b \frac{\partial \phi_y(x, y)}{\partial y} \sin(\omega_j t) \cos(\alpha_m x) \cos(\beta_n y) dx dy + K_s A_{44} \int_0^a \int_0^b \frac{\partial^2 W(x, y)}{\partial y^2} \sin(\omega_j t) \cos(\alpha_m x) \cos(\beta_n y) dx dy \\
& - \rho_1 \int_0^a \int_0^b W(x, y) \frac{\partial^2 \sin(\omega_j t)}{\partial t^2} \cos(\alpha_m x) \cos(\beta_n y) dx dy = 0
\end{aligned} \tag{12}$$

$$\begin{aligned}
& D_{11} \int_0^a \int_0^b \frac{\partial^2 \phi_x(x, y)}{\partial x^2} \sin(\omega_j t) \sin(\alpha_m x) \cos(\beta_n y) dx dy + D_{66} \int_0^a \int_0^b \frac{\partial^2 \phi_x(x, y)}{\partial y^2} \sin(\omega_j t) \sin(\alpha_m x) \cos(\beta_n y) dx dy \\
& + (D_{12} + D_{66}) \int_0^a \int_0^b \frac{\partial^2 \phi_y(x, y)}{\partial x \partial y} \sin(\omega_j t) \sin(\alpha_m x) \cos(\beta_n y) dx dy - K_s A_{55} \int_0^a \int_0^b \phi_x(x, y) \sin(\omega_j t) \sin(\alpha_m x) \cos(\beta_n y) dx dy \\
& - K_s A_{55} \int_0^a \int_0^b \frac{\partial W(x, y)}{\partial x} \sin(\omega_j t) \sin(\alpha_m x) \cos(\beta_n y) dx dy - \rho_2 \int_0^a \int_0^b \phi_x(x, y) \frac{\partial^2 \sin(\omega_j t)}{\partial t^2} \sin(\alpha_m x) \cos(\beta_n y) dx dy = 0
\end{aligned} \tag{13}$$

$$\begin{aligned}
& (D_{12} + D_{66}) \int_0^a \int_0^b \frac{\partial^2 \phi_x(x, y)}{\partial x \partial y} \sin(\omega_j t) \cos(\alpha_m x) \sin(\beta_n y) dx dy + D_{66} \int_0^a \int_0^b \frac{\partial^2 \phi_y(x, y)}{\partial x^2} \sin(\omega_j t) \cos(\alpha_m x) \sin(\beta_n y) dx dy \\
& + D_{22} \int_0^a \int_0^b \frac{\partial^2 \phi_y(x, y)}{\partial y^2} \sin(\omega_j t) \cos(\alpha_m x) \sin(\beta_n y) dx dy - K_s A_{44} \int_0^a \int_0^b \phi_y(x, y) \sin(\omega_j t) \cos(\alpha_m x) \sin(\beta_n y) dx dy \\
& - K_s A_{44} \int_0^a \int_0^b \frac{\partial W(x, y)}{\partial y} \sin(\omega_j t) \cos(\alpha_m x) \sin(\beta_n y) dx dy - \rho_2 \int_0^a \int_0^b \phi_y(x, y) \frac{\partial^2 \sin(\omega_j t)}{\partial t^2} \cos(\alpha_m x) \sin(\beta_n y) dx dy = 0
\end{aligned} \tag{14}$$

Considering the boundary conditions  $\phi_x = 0$  at  $x = \{0, a\}$  and  $\phi_y = 0$  at  $y = \{0, b\}$ , solving the three sets of dynamic equations of motions presented in Eqs. (12)–(14) leads to Eqs. (15)–(17), respectively:

$$\begin{aligned}
& K_s A_{55} (-1)^m \int_0^b \left[ \phi_x(x, y) \Big|_{x=a} \cos(\beta_n y) dy \right] - K_s A_{55} \int_0^b \left[ \phi_x(x, y) \Big|_{x=0} \cos(\beta_n y) dy \right] \\
& + K_s A_{55} (-1)^m \int_0^b \left[ \frac{\partial W(x, y)}{\partial x} \Big|_{x=a} \cos(\beta_n y) dy \right] - K_s A_{55} \int_0^b \left[ \frac{\partial W(x, y)}{\partial x} \Big|_{x=0} \cos(\beta_n y) dy \right] \\
& + K_s A_{44} (-1)^n \int_0^a \left[ \phi_y(x, y) \Big|_{y=b} \cos(\alpha_m x) dx \right] - K_s A_{44} \int_0^a \left[ \phi_y(x, y) \Big|_{y=0} \cos(\alpha_m x) dx \right] \\
& + K_s A_{44} (-1)^n \int_0^a \left[ \frac{\partial W(x, y)}{\partial y} \Big|_{y=b} \cos(\alpha_m x) dy \right] - K_s A_{44} \int_0^a \left[ \frac{\partial W(x, y)}{\partial y} \Big|_{y=0} \cos(\alpha_m x) dy \right] \\
& + K_s A_{55} \alpha_m \bar{\phi}_x(m, n) - K_s A_{55} \alpha_m^2 w(m, n) + K_s A_{44} \beta_n \bar{\phi}_y(m, n) - K_s A_{44} \beta_n^2 w(m, n) + \rho_1 \omega_j^2 w(m, n) = 0
\end{aligned} \tag{15}$$

$$\begin{aligned}
& -D_{11} \alpha_m (-1)^m \int_0^b \left[ \phi_x(x, y) \Big|_{x=a} \cos(\beta_n y) dy \right] + D_{11} \alpha_m \int_0^b \left[ \phi_x(x, y) \Big|_{x=0} \cos(\beta_n y) dy \right] \\
& + D_{66} (-1)^n \int_0^a \left[ \frac{\partial \phi_x(x, y)}{\partial y} \Big|_{y=b} \sin(\alpha_m x) dx \right] - D_{66} \int_0^a \left[ \frac{\partial \phi_x(x, y)}{\partial y} \Big|_{y=0} \sin(\alpha_m x) dx \right] \\
& - (D_{12} + D_{66}) \alpha_m (-1)^n \int_0^a \left[ \phi_y(x, y) \Big|_{y=b} \cos(\alpha_m x) dx \right] + (D_{12} + D_{66}) \alpha_m \int_0^a \left[ \phi_y(x, y) \Big|_{y=0} \cos(\alpha_m x) dx \right] \\
& - D_{11} \alpha_m^2 \bar{\phi}_x(m, n) - D_{66} \beta_n^2 \bar{\phi}_x(m, n) - (D_{12} + D_{66}) \alpha_m \beta_n \bar{\phi}_y(m, n) - K_s A_{55} \bar{\phi}_x(m, n) + K_s A_{55} \alpha_m w(m, n) \\
& + \rho_2 \omega_j^2 \bar{\phi}_x(m, n) = 0
\end{aligned} \tag{16}$$

$$\begin{aligned}
& -(D_{12} + D_{66})\beta_n (-1)^m \int_0^b \left[ \phi_x(x, y) \Big|_{x=a} \cos(\beta_n y) dy \right] + (D_{12} + D_{66})\beta_n \int_0^b \left[ \phi_x(x, y) \Big|_{x=0} \cos(\beta_n y) dy \right] \\
& + D_{66} (-1)^m \int_0^b \left[ \frac{\partial \phi_y(x, y)}{\partial x} \Big|_{x=a} \sin(\beta_n y) dy \right] - D_{66} \int_0^b \left[ \frac{\partial \phi_y(x, y)}{\partial x} \Big|_{x=0} \sin(\beta_n y) dy \right] \\
& - D_{22}\beta_n (-1)^n \int_0^a \left[ \phi_y(x, y) \Big|_{y=b} \cos(\alpha_m x) dx \right] + D_{22}\beta_n \int_0^a \left[ \phi_y(x, y) \Big|_{y=0} \cos(\alpha_m x) dx \right] \\
& - (D_{12} + D_{66})\alpha_m \beta_n \bar{\phi}_x(m, n) - D_{66}\alpha_m^2 \bar{\phi}_y(m, n) - D_{22}\beta_n^2 \bar{\phi}_y(m, n) - K_s A_{44} \bar{\phi}_y(m, n) + K_s A_{44} \beta_n w(m, n) \\
& + \rho_2 \omega_j^2 \bar{\phi}_y(m, n) = 0
\end{aligned} \tag{17}$$

In the next step, the following boundary conditions  $M_{xy} = \phi_x = 0$  at  $x = \{0, a\}$ , and  $\phi_y = 0$  at  $y = \{0, b\}$ , which are associated with a free plate, are substituted into Eqs. (15)–(17). Through mathematical procedures, a relationship between the transverse shear and vertical displacement in a dynamically excited free thick composite slab is obtained as given by Eq. (18):

To simplify the lengthy equations, the following variables are defined as:

$$I(m) = \int_0^a \left[ \phi_y(x, y) \Big|_{y=b} \cos(\alpha_m x) dx \right] \tag{23}$$

$$w(m, n) = \left[ \frac{K_s A_{55} \alpha_m}{K_s A_{55} \alpha_m^2 + K_s A_{44} \beta_n^2 - \rho_1 \omega_j^2} \right] \bar{\phi}_x(m, n) + \left[ \frac{K_s A_{44} \beta_n}{K_s A_{55} \alpha_m^2 + K_s A_{44} \beta_n^2 - \rho_1 \omega_j^2} \right] \bar{\phi}_y(m, n) \tag{18}$$

Considering the twisting deformation compatibility condition within the elastic domain at the edges:  $M_{xy} = 0$  at  $x = \{0, a\}$  and  $y = \{0, b\}$ , Eqs. (19)–(22) are derived:

$$J(m) = \int_0^a \left[ \phi_y(x, y) \Big|_{y=0} \cos(\alpha_m x) dx \right] \tag{24}$$

$$\begin{aligned}
& \left( \frac{1}{\alpha_m} \right) \int_0^a \left[ \frac{\partial \phi_x(x, y)}{\partial y} \Big|_{y=0} \sin(\alpha_m x) dx \right] - \int_0^a \left[ \phi_y(x, y) \Big|_{y=0} \cos(\alpha_m x) dx \right] \\
& = 0
\end{aligned} \tag{19}$$

$$T(n) = \int_0^b \left[ \phi_x(x, y) \Big|_{x=a} \cos(\beta_n y) dy \right] \tag{25}$$

$$\begin{aligned}
& \left( \frac{1}{\alpha_m} \right) \int_0^a \left[ \frac{\partial \phi_x(x, y)}{\partial y} \Big|_{y=b} \sin(\alpha_m x) dx \right] - \int_0^a \left[ \phi_y(x, y) \Big|_{y=b} \cos(\alpha_m x) dx \right] \\
& = 0
\end{aligned} \tag{20}$$

$$L(n) = \int_0^b \left[ \phi_x(x, y) \Big|_{x=0} \cos(\beta_n y) dy \right] \tag{26}$$

$$\begin{aligned}
& \left( \frac{1}{\beta_n} \right) \int_0^b \left[ \frac{\partial \phi_y(x, y)}{\partial x} \Big|_{x=0} \sin(\beta_n y) dy \right] - \int_0^b \left[ \phi_x(x, y) \Big|_{x=0} \cos(\beta_n y) dy \right] \\
& = 0
\end{aligned} \tag{21}$$

$$\zeta_1(m, n, \omega_j) = \frac{K_s A_{55} \alpha_m}{K_s A_{55} \alpha_m^2 + K_s A_{44} \beta_n^2 - \rho_1 \omega_j^2} \tag{27}$$

$$\zeta_2(m, n, \omega_j) = \frac{K_s A_{44} \beta_n}{K_s A_{55} \alpha_m^2 + K_s A_{44} \beta_n^2 - \rho_1 \omega_j^2} \tag{28}$$

$$\begin{aligned}
& \left( \frac{1}{\beta_n} \right) \int_0^b \left[ \frac{\partial \phi_y(x, y)}{\partial x} \Big|_{x=a} \sin(\beta_n y) dy \right] - \int_0^b \left[ \phi_x(x, y) \Big|_{x=a} \cos(\beta_n y) dy \right] \\
& = 0
\end{aligned} \tag{22}$$

where, the terms  $I(m)$ ,  $J(m)$ ,  $T(n)$ , and  $L(n)$  denote four Fourier integral equations, depending on representing Fourier variables;  $\zeta_1$  and  $\zeta_2$  stand for two unknown nonlinear frequency functions which are dependent on the eigenfrequency and the transverse shear stiffness in a suspended thick composite slab under harmonic motion. Substituting Eqs. (19)–(26) into Eq. (16) and Eq. (17) leads to Eq. (29) and Eq. (30), respectively:

$$\begin{aligned}
& D_{12}\alpha_m (-1)^n I(m) - D_{12}\alpha_m J(m) + D_{11}\alpha_m (-1)^m T(n) - D_{11}\alpha_m L(n) - K_s A_{55} \alpha_m w(m, n) \\
& + \left( D_{11}\alpha_m^2 + D_{66}\beta_n^2 + K_s A_{55} - \rho_2 \omega_j^2 \right) \bar{\phi}_x(m, n) + (D_{12} + D_{66})\alpha_m \beta_n \bar{\phi}_y(m, n) = 0
\end{aligned} \tag{29}$$

$$D_{22}\beta_n(-1)^n I(m) - D_{22}\beta_n J(m) + D_{12}(-1)^m T(n) - D_{12}\beta_n L(n) - K_s A_{44}\beta_n w(m, n) + (D_{12} + D_{66})\alpha_m \beta_n \bar{\phi}_x(m, n) + (D_{66}\alpha_m^2 + D_{22}\beta_n^2 + K_s A_{44} - \rho_2 \omega_j^2) \bar{\phi}_y(m, n) = 0 \tag{30}$$

Substitution of Eq. (18) into Eq. (29) and Eq. (30) leads to a constitutive matrix equation, describing the relationship between the lateral deflection and transverse shear deformation and four Fourier integral equations and two nonlinear frequency functions, as given by Eq. (31):

$$\begin{bmatrix} w(m, n, \omega_j) \\ \bar{\phi}_x(m, n, \omega_j) \\ \bar{\phi}_y(m, n, \omega_j) \end{bmatrix} = \begin{bmatrix} V_{11}(m, n, \omega_j) & V_{12}(m, n, \omega_j) & V_{13}(m, n, \omega_j) & V_{14}(m, n, \omega_j) \\ V_{21}(m, n, \omega_j) & V_{22}(m, n, \omega_j) & V_{23}(m, n, \omega_j) & V_{24}(m, n, \omega_j) \\ V_{31}(m, n, \omega_j) & V_{32}(m, n, \omega_j) & V_{33}(m, n, \omega_j) & V_{34}(m, n, \omega_j) \end{bmatrix} \begin{bmatrix} I(m) \\ J(m) \\ T(n) \\ L(n) \end{bmatrix} \tag{31}$$

where, the matrix elements  $V_{ij}(m, n, \omega_j)$  can be found in Appendix A.

The bending deformations  $M_x$  and  $M_y$  in a suspended thick composite slab are derived using the differentiation approach associated with higher order series as:

$$M_x(x, y) = D_{11} \frac{\partial \phi_x(x, y)}{\partial x} + D_{12} \frac{\partial \phi_y(x, y)}{\partial y} = \frac{2D_{11}}{ab} \sum_{m=0}^{\infty} \sum_{n=0}^{\infty} \Delta_m \Delta_n \left( (-1)^m \int_0^b \left[ \phi_x(x, y) \Big|_{x=a} \cos(\beta_n y) dy \right] - \int_0^b \left[ \phi_x(x, y) \Big|_{x=0} \cos(\beta_n y) dy \right] + \alpha_m \bar{\phi}_x(m, n, \omega_j) \right) \cos(\alpha_m x) \cos(\beta_n y) + \frac{2D_{12}}{ab} \sum_{m=0}^{\infty} \sum_{n=0}^{\infty} \Delta_m \Delta_n \left( (-1)^n \int_0^a \left[ \phi_y(x, y) \Big|_{y=b} \cos(\alpha_m x) dx \right] - \int_0^a \left[ \phi_y(x, y) \Big|_{y=0} \cos(\alpha_m x) dx \right] + \beta_n \bar{\phi}_y(m, n, \omega_j) \right) \cos(\alpha_m x) \cos(\beta_n y) \tag{32}$$

$$M_y(x, y) = D_{12} \frac{\partial \phi_x(x, y)}{\partial x} + D_{22} \frac{\partial \phi_y(x, y)}{\partial y} = \frac{2D_{12}}{ab} \sum_{m=0}^{\infty} \sum_{n=0}^{\infty} \Delta_m \Delta_n \left( (-1)^m \int_0^b \left[ \phi_x(x, y) \Big|_{x=a} \cos(\beta_n y) dy \right] - \int_0^b \left[ \phi_x(x, y) \Big|_{x=0} \cos(\beta_n y) dy \right] + \alpha_m \bar{\phi}_x(m, n, \omega_j) \right) \cos(\alpha_m x) \cos(\beta_n y) + \frac{2D_{22}}{ab} \sum_{m=0}^{\infty} \sum_{n=0}^{\infty} \Delta_m \Delta_n \left( (-1)^n \int_0^a \left[ \phi_y(x, y) \Big|_{y=b} \cos(\alpha_m x) dx \right] - \int_0^a \left[ \phi_y(x, y) \Big|_{y=0} \cos(\alpha_m x) dx \right] + \beta_n \bar{\phi}_y(m, n, \omega_j) \right) \cos(\alpha_m x) \cos(\beta_n y) \tag{33}$$

where,  $\Delta_m = 1$  for  $m = 0$ ,  $\Delta_m = 2$  for  $m = \{1, 2, 3, \dots, \infty\}$ ,  $\Delta_n = 1$  for  $n = 0$ , and  $\Delta_n = 2$  for  $n = \{1, 2, 3, \dots, \infty\}$ . Eq. (32) and Eq. (33) leads to Eqs. (34)–(37), respectively, due to the fact that ( $M_x = 0$  at  $x = \{0, a\}$  and  $M_y = 0$  at  $y = \{0, b\}$ ):

$$D_{12} \sum_{m=0}^{\infty} \sum_{n=0}^{\infty} \Delta_m \Delta_n (-1)^n I(m) \cos(\beta_n y) - D_{12} \sum_{m=0}^{\infty} \sum_{n=0}^{\infty} \Delta_m \Delta_n J(m) \cos(\beta_n y) + D_{11} \sum_{m=0}^{\infty} \sum_{n=0}^{\infty} \Delta_m \Delta_n (-1)^m T(n) \cos(\beta_n y) - D_{11} \sum_{m=0}^{\infty} \sum_{n=0}^{\infty} \Delta_m \Delta_n L(n) \cos(\beta_n y) + D_{11} \sum_{m=0}^{\infty} \sum_{n=0}^{\infty} \Delta_m \Delta_n \alpha_m \bar{\phi}_x(m, n, \omega_j) \cos(\beta_n y) + D_{12} \sum_{m=0}^{\infty} \sum_{n=0}^{\infty} \Delta_m \Delta_n \beta_n \bar{\phi}_y(m, n, \omega_j) \cos(\beta_n y) = 0 \tag{34}$$

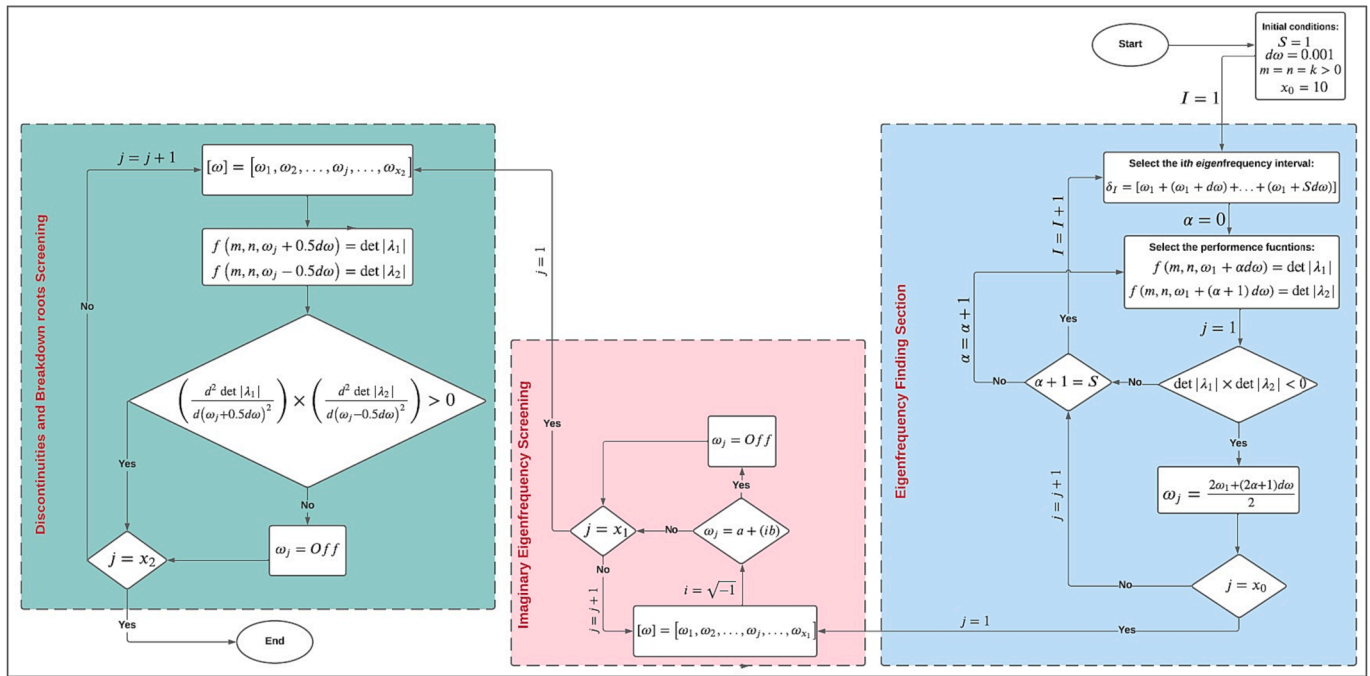


Fig. 2. The proposed algorithm for the calculation of the eigenfrequencies of suspended slabs with the capability to distinguish the real roots from the unacceptable roots of eigenvalues.

$$\begin{aligned}
 & D_{12} \sum_{m=0}^{\infty} \sum_{n=0}^{\infty} \Delta_m \Delta_n (-1)^m (-1)^n I(m) \cos(\beta_n y) - D_{12} \sum_{m=0}^{\infty} \sum_{n=0}^{\infty} \Delta_m \Delta_n (-1)^m J(m) \cos(\beta_n y) \\
 & + D_{11} \sum_{m=0}^{\infty} \sum_{n=0}^{\infty} \Delta_m \Delta_n (-1)^{2m} T(n) \cos(\beta_n y) - D_{11} \sum_{m=0}^{\infty} \sum_{n=0}^{\infty} \Delta_m \Delta_n (-1)^m L(n) \cos(\beta_n y) \\
 & + D_{11} \sum_{m=0}^{\infty} \sum_{n=0}^{\infty} \Delta_m \Delta_n \alpha_m (-1)^m \bar{\phi}_x(m, n, \omega_j) \cos(\beta_n y) + D_{12} \sum_{m=0}^{\infty} \sum_{n=0}^{\infty} \Delta_m \Delta_n \beta_n (-1)^m \bar{\phi}_y(m, n, \omega_j) \cos(\beta_n y) = 0
 \end{aligned} \tag{35}$$

$$\begin{aligned}
 & D_{22} \sum_{m=0}^{\infty} \sum_{n=0}^{\infty} \Delta_m \Delta_n (-1)^n I(m) \cos(\alpha_m x) - D_{22} \sum_{m=0}^{\infty} \sum_{n=0}^{\infty} \Delta_m \Delta_n J(m) \cos(\alpha_m x) \\
 & + D_{12} \sum_{m=0}^{\infty} \sum_{n=0}^{\infty} \Delta_m \Delta_n (-1)^m T(n) \cos(\alpha_m x) - D_{12} \sum_{m=0}^{\infty} \sum_{n=0}^{\infty} \Delta_m \Delta_n L(n) \cos(\alpha_m x) \\
 & + D_{12} \sum_{m=0}^{\infty} \sum_{n=0}^{\infty} \Delta_m \Delta_n \alpha_m \bar{\phi}_x(m, n, \omega_j) \cos(\alpha_m x) + D_{22} \sum_{m=0}^{\infty} \sum_{n=0}^{\infty} \Delta_m \Delta_n \beta_n \bar{\phi}_y(m, n, \omega_j) \cos(\alpha_m x) = 0
 \end{aligned} \tag{36}$$

$$\begin{aligned}
 & D_{22} \sum_{m=0}^{\infty} \sum_{n=0}^{\infty} \Delta_m \Delta_n (-1)^{2n} I(m) \cos(\alpha_m x) - D_{22} \sum_{m=0}^{\infty} \sum_{n=0}^{\infty} \Delta_m \Delta_n (-1)^n J(m) \cos(\alpha_m x) \\
 & + D_{12} \sum_{m=0}^{\infty} \sum_{n=0}^{\infty} \Delta_m \Delta_n (-1)^m (-1)^n T(n) \cos(\alpha_m x) - D_{12} \sum_{m=0}^{\infty} \sum_{n=0}^{\infty} \Delta_m \Delta_n (-1)^n L(n) \cos(\alpha_m x) \\
 & + D_{12} \sum_{m=0}^{\infty} \sum_{n=0}^{\infty} \Delta_m \Delta_n \alpha_m (-1)^n \bar{\phi}_x(m, n, \omega_j) \cos(\alpha_m x) + D_{22} \sum_{m=0}^{\infty} \sum_{n=0}^{\infty} \Delta_m \Delta_n \beta_n (-1)^n \bar{\phi}_y(m, n, \omega_j) \cos(\alpha_m x) = 0
 \end{aligned} \tag{37}$$

The analytical solution to the free vibration problem of a laminated composite slab can be formulated by considering the principles of higher-order trigonometric series, the transverse shear deformation, and four Fourier integral equations in Eq. (31). A set of four trigonometric

series-based analytical equations containing the natural frequencies of free vibration, flexural stiffness associated with an orthotropic material, and four Fourier integral variables  $I(m)$ ,  $J(m)$ ,  $T(n)$ , and  $L(n)$  are derived as

**Table 1**

The engineering constants of several isotropic and composite materials used in the present study.

Material properties	Aluminum [15,16]	Graphite epoxy GFRP [37,38]	T300/914 CFRP [39]	T300/976 CFRP [40,41,42]
$E_1$ (GPa)	69	40	10.20	150
$E_2$ (GPa)	69	1	10.20	9
$E_3$ (GPa)	69	1	5.50	9
$\nu_{12}$	0.3	0.25	0.183	0.3
$\nu_{13}$	0.3	0.25	0.512	0.3
$\nu_{23}$	0.3	0.25	0.512	0.3
$G_{12}$ (GPa)	26.5	0.6	1.58	7.1
$G_{13}$ (GPa)	26.5	0.6	1.56	7.1
$G_{23}$ (GPa)	26.5	0.5	1.56	2.5
$\rho$ (Kg/m <sup>3</sup> )	2707	1000	1520	1600

**Table 2**

The engineering constants of various types of CFRP composites used in the present study.

Material properties	CFRP.1 [43]	CFRP.2 [44]	CFRP.3 [35]	CFRP.4 [45]	CFRP.5 [35]
$E_1$ (GPa)	128	138	139	168.98	150
$E_2$ (GPa)	11	8.96	8.76	9.05	10
$G_{12}$ (GPa)	4.5	7.1	4.57	5	5
$\nu_{12}$	0.25	0.30	0.32	0.288	0.30

$$\begin{aligned}
 & \sum_{m=0}^{\infty} \Delta_m \Delta_n [D_{12}(-1)^n + D_{11}\alpha_m V_{21}(m, n, \omega_j) + D_{12}\beta_n V_{31}(m, n, \omega_j)] I(m) \\
 & + \sum_{m=0}^{\infty} \Delta_m \Delta_n [D_{11}\alpha_m V_{22}(m, n, \omega_j) + D_{12}\beta_n V_{32}(m, n, \omega_j) - D_{12}] J(m) \\
 & + \sum_{m=0}^{\infty} \Delta_m \Delta_n [D_{11}(-1)^m + D_{11}\alpha_m V_{23}(m, n, \omega_j) + D_{12}\beta_n V_{33}(m, n, \omega_j)] T(n) \\
 & + \sum_{m=0}^{\infty} \Delta_m \Delta_n [D_{11}\alpha_m V_{24}(m, n, \omega_j) + D_{12}\beta_n V_{34}(m, n, \omega_j) - D_{11}] L(n) = 0
 \end{aligned} \tag{38}$$

$$\begin{aligned}
 & \sum_{m=0}^{\infty} \Delta_m \Delta_n [D_{12}(-1)^m (-1)^n + D_{11}\alpha_m (-1)^m V_{21}(m, n, \omega_j) + D_{12}\beta_n (-1)^m V_{31}(m, n, \omega_j)] I(m) \\
 & + \sum_{m=0}^{\infty} \Delta_m \Delta_n [D_{11}\alpha_m (-1)^m V_{22}(m, n, \omega_j) + D_{12}\beta_n (-1)^m V_{32}(m, n, \omega_j) - D_{12}(-1)^m] J(m) \\
 & + \sum_{m=0}^{\infty} \Delta_m \Delta_n [D_{11}(-1)^{2m} + D_{11}\alpha_m (-1)^m V_{23}(m, n, \omega_j) + D_{12}\beta_n (-1)^m V_{33}(m, n, \omega_j)] T(n) \\
 & + \sum_{m=0}^{\infty} \Delta_m \Delta_n [D_{11}\alpha_m (-1)^m V_{24}(m, n, \omega_j) + D_{12}\beta_n (-1)^m V_{34}(m, n, \omega_j) - D_{11}(-1)^m] L(n) = 0
 \end{aligned} \tag{39}$$

**Table 3**

The effect of different Poisson's ratios on the first three natural frequencies of the suspended square plate slab made of aluminum and with the constant total thickness of  $H = 3$  (mm).

Method		Non-dimensional natural frequency: $\Psi_j$		
		1	2	3
$\nu = 0.225$	HMN [16]	14.116	20.387	23.878
	FEM [16]	14.126	20.396	23.886
	Analytical [15]	14.14	20.49	23.97
	Present (n = m = 5)	13.477	20.524	23.871
	Present (n = m = 10)	13.829	20.348	23.871
	Present (n = m = 15)	13.829	20.348	23.871
$\nu = 0.3$	HMN [16]	13.468	19.596	24.270
	FEM [16]	13.472	19.600	24.273
	Analytical [15]	13.4728	19.5961	24.2702
	Present (n = m = 5)	12.850	24.234	59.420
	Present (n = m = 10)	13.195	19.577	24.234
	Present (n = m = 15)	13.195	19.577	24.234
$\nu = 0.343$	HMN [16]	13.076	19.108	24.467
	FEM [16]	13.074	19.108	24.467
	Analytical [15]	13.086	19.231	24.58
	Present (n = m = 5)	12.493	19.178	24.477
	Present (n = m = 10)	12.738	19.097	24.437
	Present (n = m = 15)	12.860	19.097	24.437
$\nu = 0.360$	HMN [16]	12.916	18.907	24.538
	FEM [16]	12.919	18.911	24.541
	Analytical [15]	12.927	19.045	24.66
	Present (n = m = 5)	12.327	18.967	24.514
	Present (n = m = 10)	12.570	18.886	24.514
	Present (n = m = 15)	12.692	18.886	24.514
$\nu = 390$	HMN [16]	12.628	18.542	24.654
	FEM [16]	12.628	18.543	24.654
	Analytical [15]	12.64	18.707	24.80
	Present (n = m = 5)	12.047	18.600	24.594
	Present (n = m = 10)	12.287	18.520	24.594
	Present (n = m = 15)	12.407	18.520	24.634
Present (n = m = 20)	12.447	18.520	24.634	

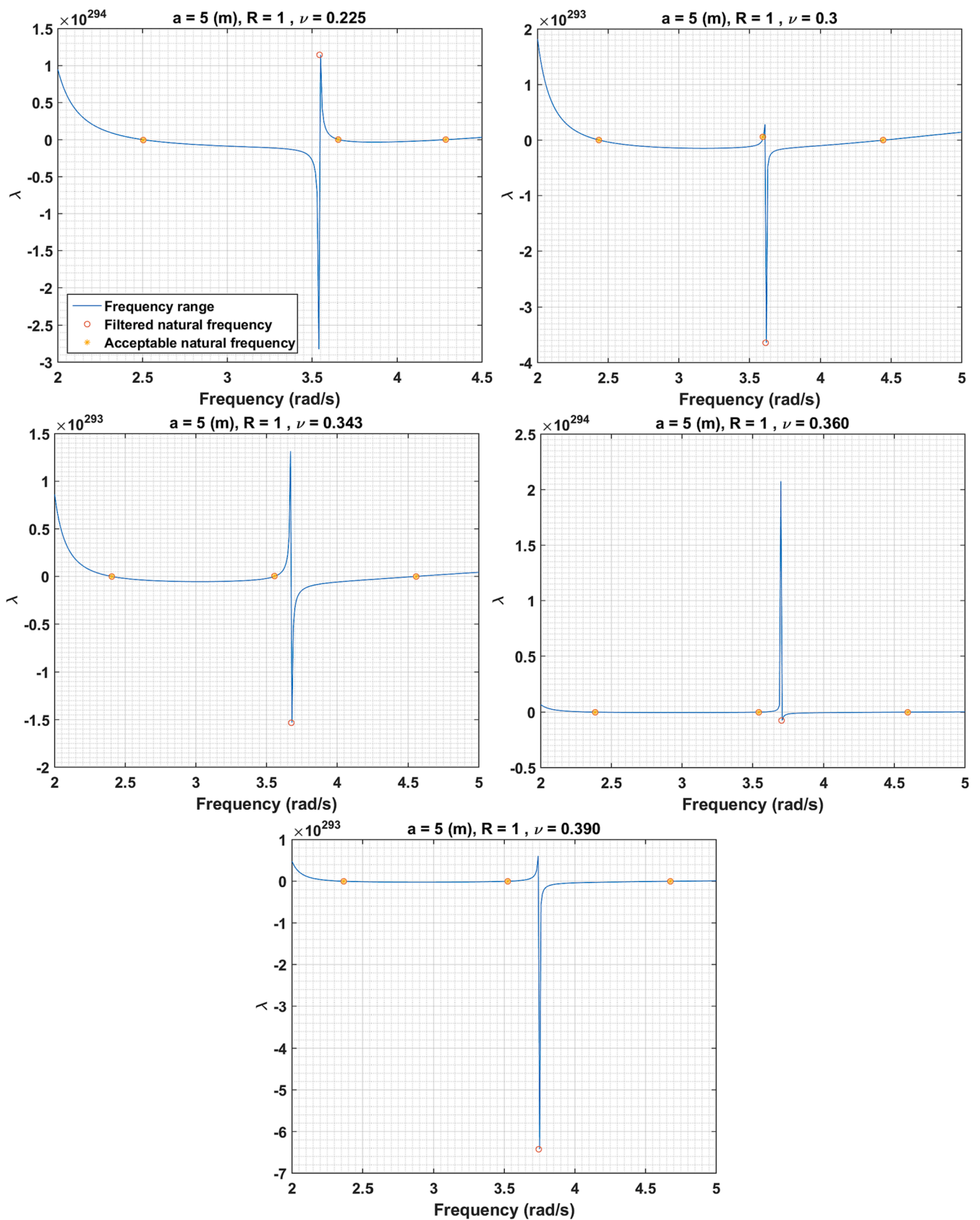


Fig. 3. The use of the proposed algorithm in Table.2 to detect the real roots of the eigenfrequency matrix and distinguish them from the unacceptable roots.

**Table 4**

The effect of geometrical dimension on the first ten natural frequencies of the suspended plate slab made of aluminum and with the constant total thickness of  $H = 3$  (mm).

$\left(\frac{b}{a}\right)$	Method	Non-dimensional natural frequency: $\Psi_j$									
		1	2	3	4	5	6	7	8	9	10
1.5	HMN [16]	8.931	9.517	20.599	22.182	25.650	29.791	38.158	43.926	53.346	60.046
	FEM [16]	8.931	9.517	20.599	22.183	25.652	29.792	38.159	43.928	53.353	60.054
	Present	8.819	9.514	20.306	22.169	25.547	29.633	37.652	43.298	53.283	59.765
2	HMN [16]	5.365	6.643	14.621	14.902	22.002	25.376	26.001	29.681	36.045	40.050
	FEM [16]	5.365	6.643	14.620	14.902	22.003	25.376	26.001	29.684	36.046	40.052
	Present	5.362	6.563	14.412	14.888	21.987	24.993	25.845	29.637	35.631	39.527
2.5	HMN [16]	3.432	5.278	9.540	11.329	18.627	18.923	22.447	24.444	28.750	31.450
	FEM [16]	3.432	5.278	9.540	11.328	18.628	18.923	22.448	24.445	28.750	31.450
	Present	3.432	5.217	9.535	11.172	18.612	18.626	22.432	24.332	28.325	31.134
3	HMN [16]	2.382	4.375	6.616	9.244	13.026	15.073	21.312	22.227	22.289	24.348
	FEM [16]	2.381	4.375	6.616	9.243	13.026	15.072	21.313	22.228	22.289	24.348
	Present	2.382	4.328	6.613	9.121	13.017	14.838	21.288	21.942	22.211	24.268
3.5	HMN [16]	1.748	3.736	4.853	7.806	9.565	12.522	15.846	18.164	21.979	23.500
	FEM [16]	1.747	3.736	4.853	7.806	9.565	12.522	15.847	18.163	21.980	23.501
	Present	1.749	3.694	4.853	7.705	9.560	12.334	15.840	17.877	21.962	23.428
4	HMN [16]	1.338	3.259	3.711	6.757	7.314	10.711	12.136	15.317	18.124	20.751
	FEM [16]	1.337	3.260	3.710	6.757	7.314	10.710	12.136	15.317	18.125	20.750
	Present	1.339	3.222	3.711	6.675	7.312	10.554	12.131	15.078	18.117	20.406
4.5	HMN [16]	1.056	2.891	2.928	5.771	5.957	9.359	9.580	13.240	14.346	17.730
	FEM [16]	1.055	2.891	2.928	5.771	5.957	9.358	9.580	12.240	14.346	17.729
	Present	1.057	2.858	2.928	5.768	5.884	9.229	9.577	13.037	14.345	17.434
5	HMN [16]	0.855	2.369	2.597	4.668	5.327	7.750	8.312	11.615	11.660	15.471
	FEM [16]	0.855	2.369	2.597	4.669	5.327	7.750	8.311	11.615	11.660	15.470
	Present	0.854	2.369	2.568	4.667	5.263	7.751	8.198	11.485	11.613	15.215

$$\begin{aligned}
 & \sum_{n=0}^{\infty} \Delta_m \Delta_n [D_{22}(-1)^n + D_{12}\alpha_m V_{21}(m, n, \omega_j) + D_{22}\beta_n V_{31}(m, n, \omega_j)] I(m) \\
 & + \sum_{n=0}^{\infty} \Delta_m \Delta_n [D_{12}\alpha_m V_{22}(m, n, \omega_j) + D_{22}\beta_n V_{32}(m, n, \omega_j) - D_{22}] J(m) \\
 & + \sum_{n=0}^{\infty} \Delta_m \Delta_n [D_{12}(-1)^m + D_{12}\alpha_m V_{23}(m, n, \omega_j) + D_{22}\beta_n V_{33}(m, n, \omega_j)] T(n) \\
 & + \sum_{n=0}^{\infty} \Delta_m \Delta_n [D_{12}\alpha_m V_{24}(m, n, \omega_j) + D_{22}\beta_n V_{34}(m, n, \omega_j) - D_{12}] L(n) = 0
 \end{aligned}
 \tag{40}$$

The Fourier terms  $m$  and  $n$  can be used for the convergence analysis. The accuracy of the results associated with natural frequencies of free vibration can be improved by selecting the higher values for the Fourier terms  $m$  and  $n$ .

Eqs. (38)–(41) are rearranged to form a constitutive equation of motion which is expressed as:

$$[\lambda][V] = 0 \tag{42}$$

where, the eigenfrequency matrix  $[\lambda]$  and an eigenvector  $[V]$  are expressed by Eq. (43) and Eq. (44), respectively:

$$\begin{aligned}
 & \sum_{n=0}^{\infty} \Delta_m \Delta_n [D_{22}(-1)^{2n} + D_{12}\alpha_m(-1)^n V_{21}(m, n, \omega_j) + D_{22}\beta_n(-1)^n V_{31}(m, n, \omega_j)] I(m) \\
 & + \sum_{n=0}^{\infty} \Delta_m \Delta_n [D_{12}\alpha_m(-1)^n V_{22}(m, n, \omega_j) + D_{22}\beta_n(-1)^n V_{32}(m, n, \omega_j) - D_{22}(-1)^n] J(m) \\
 & + \sum_{n=0}^{\infty} \Delta_m \Delta_n [D_{12}(-1)^m(-1)^n + D_{12}\alpha_m(-1)^n V_{23}(m, n, \omega_j) + D_{22}\beta_n(-1)^n V_{33}(m, n, \omega_j)] T(n) \\
 & + \sum_{n=0}^{\infty} \Delta_m \Delta_n [D_{12}\alpha_m(-1)^n V_{24}(m, n, \omega_j) + D_{22}\beta_n(-1)^n V_{34}(m, n, \omega_j) - D_{12}(-1)^n] L(n) = 0
 \end{aligned}
 \tag{41}$$

**Table 5**

The effect of geometrical dimension on the first ten natural frequencies of the suspended plate slab made of a composite material with the following flexural properties: ( $D_{22} = 2D_{11}$ ,  $D_{12} = 0.3D_{11}$ , and  $D_{66} = D_{11} - 0.5D_{12}$ ).

$\left(\frac{b}{a}\right)$	Method	Non-dimensional natural frequency: $\Psi_j$									
		1	2	3	4	5	6	7	8	9	10
1	Analytical [33]	20.56	21.75	31.77	46.98	51.62	61.72	86.83	86.85	91.57	107.04
	FEM [33]	20.56	21.75	31.77	46.98	51.63	61.75	86.88	86.89	91.59	107.09
	Analytical [34]	20.56	21.75	31.76	46.98	51.62	61.72	86.83	86.84	91.57	107.03
	Present	20.29	21.77	31.77	46.35	51.04	61.73	85.74	86.79	90.32	106.16
1.5	Analytical [33]	13.70	13.71	22.38	30.93	34.94	39.05	56.35	61.28	61.39	74.16
	FEM [33]	13.70	13.73	22.39	30.93	34.95	39.09	56.38	61.29	61.42	74.20
	Analytical [34]	13.70	13.71	22.38	30.92	34.94	39.05	56.34	61.28	61.39	74.16
	Present	13.53	13.71	22.38	30.52	34.58	39.02	55.62	60.44	61.37	73.57
2	Analytical [33]	7.75	10.23	21.49	22.10	22.25	30.52	37.77	42.41	47.92	58.59
	FEM [33]	7.75	10.23	21.49	22.10	22.26	30.52	37.77	42.43	47.93	58.60
	Analytical [34]	7.75	10.23	21.49	22.10	22.25	30.52	37.77	42.41	47.92	58.59
	Present	7.75	10.11	21.48	21.81	22.25	30.26	37.23	42.39	47.33	57.90
2.5	Analytical [33]	4.96	8.15	13.76	17.21	22.16	27.26	27.74	28.34	40.36	42.55
	FEM [33]	4.96	8.15	13.77	17.22	22.17	27.28	27.76	28.35	40.38	42.58
	Analytical [34]	4.96	8.15	13.76	17.21	22.16	27.25	27.74	28.34	40.35	42.55
	Present	4.96	8.06	13.76	17.00	22.15	27.25	27.55	27.92	39.87	41.96
3	Analytical [33]	3.44	6.77	9.55	14.11	18.70	22.41	22.69	26.07	31.33	33.18
	FEM [33]	3.44	6.77	9.55	14.11	18.71	22.42	22.70	26.09	31.36	33.19
	Analytical [34]	3.44	6.77	9.55	14.11	18.70	22.41	22.69	26.07	31.33	33.18
	Present	3.44	6.69	9.55	13.93	18.69	22.37	22.40	25.93	31.34	32.69
3.5	Analytical [33]	2.53	5.79	7.01	11.96	13.78	18.94	22.31	22.68	25.43	27.17
	FEM [33]	2.53	5.79	7.01	11.96	13.78	18.94	22.32	22.69	25.44	27.18
	Analytical [34]	2.53	5.79	7.01	11.96	13.77	18.94	22.31	22.68	25.43	27.17
	Present	2.52	5.72	7.01	11.81	13.78	18.67	22.31	22.67	25.33	26.77
4	Analytical [33]	1.93	5.05	5.36	10.38	10.54	16.26	17.45	22.26	23.01	24.59
	FEM [33]	1.93	5.05	5.36	10.38	10.55	16.27	17.46	22.27	23.02	24.61
	Analytical [34]	1.93	5.05	5.36	10.38	10.54	16.26	17.45	22.26	23.01	24.59
	Present	1.94	4.99	5.36	10.25	10.54	16.05	17.46	22.25	22.68	24.50
4.5	Analytical [33]	1.53	4.23	4.49	8.33	9.17	13.79	14.26	19.97	20.54	22.43
	FEM [33]	1.53	4.23	4.49	8.33	9.17	13.80	14.26	19.98	20.56	22.44
	Analytical [34]	1.53	4.23	4.49	8.33	9.17	13.79	14.26	19.97	20.54	22.43
	Present	1.52	4.23	4.44	8.33	9.06	13.80	14.07	19.69	20.56	22.42
5	Analytical [33]	1.23	3.42	4.03	6.74	8.21	11.17	12.70	16.70	17.65	22.33
	FEM [33]	1.23	3.42	4.03	6.74	8.22	11.17	12.70	16.71	17.65	22.35
	Analytical [34]	1.23	3.42	4.03	6.74	8.21	11.17	12.70	16.70	17.65	22.33
	Present	1.23	3.43	3.99	6.74	8.12	11.17	12.53	16.71	17.40	22.33

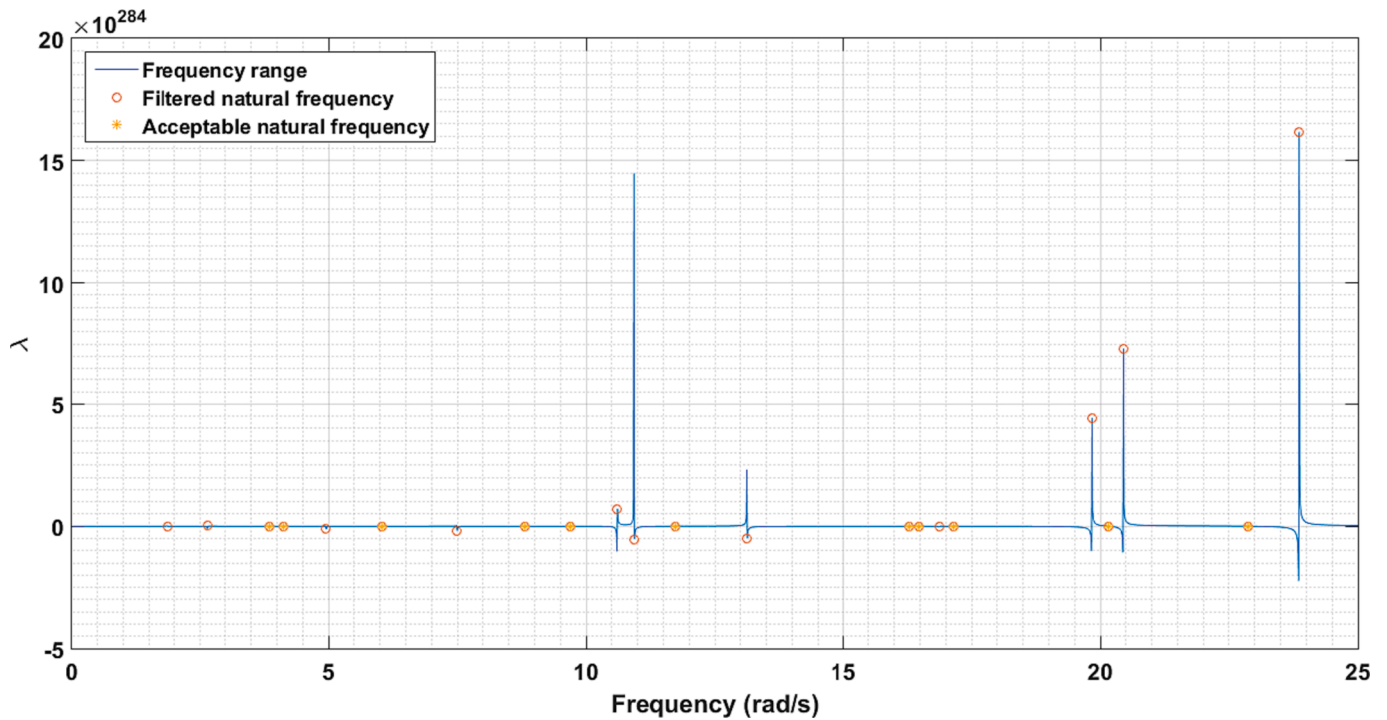


Fig. 4. The use of the proposed algorithm in Table 5 to detect the real roots of the eigenfrequency matrix and distinguish them from the unacceptable roots for a suspended square composite plate ( $R = 1$ ).

$[\lambda] =$

$$\begin{bmatrix}
 S_1(0,0,\omega_j) & S_1(1,0,\omega_j) & \dots & S_1(m,0,\omega_j) & S_2(0,0,\omega_j) & S_2(1,0,\omega_j) & \dots & S_2(m,0,\omega_j) & \bar{s}_3(0,\omega_j) & 0 & \dots & 0 & \bar{s}_4(0,\omega_j) & 0 & \dots & 0 \\
 S_1(0,1,\omega_j) & S_1(1,1,\omega_j) & \dots & S_1(m,1,\omega_j) & S_2(0,1,\omega_j) & S_2(1,1,\omega_j) & \dots & S_2(m,1,\omega_j) & 0 & \bar{s}_3(1,\omega_j) & \dots & 0 & 0 & \bar{s}_4(1,\omega_j) & \dots & 0 \\
 \vdots & \vdots & \ddots & \vdots & \vdots & \vdots & \ddots & \vdots & \vdots & \vdots & \ddots & \vdots & \vdots & \vdots & \ddots & \vdots \\
 S_1(0,n,\omega_j) & S_1(1,n,\omega_j) & \dots & S_1(m,n,\omega_j) & S_2(0,n,\omega_j) & S_2(1,n,\omega_j) & \dots & S_2(m,n,\omega_j) & 0 & 0 & \dots & \bar{s}_3(n,\omega_j) & 0 & 0 & \dots & \bar{s}_4(n,\omega_j) \\
 \hline
 S_5(0,0,\omega_j) & S_5(1,0,\omega_j) & \dots & S_5(m,0,\omega_j) & S_6(0,0,\omega_j) & S_6(1,0,\omega_j) & \dots & S_6(m,0,\omega_j) & \bar{s}_7(0,\omega_j) & 0 & \dots & 0 & \bar{s}_8(0,\omega_j) & 0 & \dots & 0 \\
 S_5(0,1,\omega_j) & S_5(1,1,\omega_j) & \dots & S_5(m,1,\omega_j) & S_6(0,1,\omega_j) & S_6(1,1,\omega_j) & \dots & S_6(m,1,\omega_j) & 0 & \bar{s}_7(1,\omega_j) & \dots & 0 & 0 & \bar{s}_8(1,\omega_j) & \dots & 0 \\
 \vdots & \vdots & \ddots & \vdots & \vdots & \vdots & \ddots & \vdots & \vdots & \vdots & \ddots & \vdots & \vdots & \vdots & \ddots & \vdots \\
 S_5(0,n,\omega_j) & S_5(1,n,\omega_j) & \dots & S_5(m,n,\omega_j) & S_6(0,n,\omega_j) & S_6(1,n,\omega_j) & \dots & S_6(m,n,\omega_j) & 0 & 0 & \dots & \bar{s}_7(n,\omega_j) & 0 & 0 & \dots & \bar{s}_8(n,\omega_j) \\
 \hline
 \bar{s}_9(0,\omega_j) & 0 & \dots & 0 & \bar{s}_{10}(0,\omega_j) & 0 & \dots & 0 & S_{11}(0,0,\omega_j) & S_{11}(0,1,\omega_j) & \dots & S_{11}(0,n,\omega_j) & S_{12}(0,0,\omega_j) & S_{12}(0,1,\omega_j) & \dots & S_{12}(0,n,\omega_j) \\
 0 & \bar{s}_9(1,\omega_j) & \dots & 0 & 0 & \bar{s}_{10}(1,\omega_j) & \dots & 0 & S_{11}(1,0,\omega_j) & S_{11}(1,1,\omega_j) & \dots & S_{11}(1,n,\omega_j) & S_{12}(1,0,\omega_j) & S_{12}(1,1,\omega_j) & \dots & S_{12}(1,n,\omega_j) \\
 \vdots & \vdots & \ddots & \vdots & \vdots & \vdots & \ddots & \vdots & \vdots & \vdots & \ddots & \vdots & \vdots & \vdots & \ddots & \vdots \\
 0 & 0 & \dots & \bar{s}_9(m,\omega_j) & 0 & 0 & \dots & \bar{s}_{10}(m,\omega_j) & S_{11}(m,0,\omega_j) & S_{11}(m,1,\omega_j) & \dots & S_{11}(m,n,\omega_j) & S_{12}(m,0,\omega_j) & S_{12}(m,1,\omega_j) & \dots & S_{12}(m,n,\omega_j) \\
 \hline
 \bar{s}_{13}(0,\omega_j) & 0 & \dots & 0 & \bar{s}_{14}(0,\omega_j) & 0 & \dots & 0 & S_{15}(0,0,\omega_j) & S_{15}(0,1,\omega_j) & \dots & S_{15}(0,n,\omega_j) & S_{16}(0,0,\omega_j) & S_{16}(0,1,\omega_j) & \dots & S_{16}(0,n,\omega_j) \\
 0 & \bar{s}_{13}(1,\omega_j) & \dots & 0 & 0 & \bar{s}_{14}(1,\omega_j) & \dots & 0 & S_{15}(1,0,\omega_j) & S_{15}(1,1,\omega_j) & \dots & S_{15}(1,n,\omega_j) & S_{16}(1,0,\omega_j) & S_{16}(1,1,\omega_j) & \dots & S_{16}(1,n,\omega_j) \\
 \vdots & \vdots & \ddots & \vdots & \vdots & \vdots & \ddots & \vdots & \vdots & \vdots & \ddots & \vdots & \vdots & \vdots & \ddots & \vdots \\
 0 & 0 & \dots & \bar{s}_{13}(m,\omega_j) & 0 & 0 & \dots & \bar{s}_{14}(m,\omega_j) & S_{15}(m,0,\omega_j) & S_{15}(m,1,\omega_j) & \dots & S_{15}(m,n,\omega_j) & S_{16}(m,0,\omega_j) & S_{16}(m,1,\omega_j) & \dots & S_{16}(m,n,\omega_j)
 \end{bmatrix} \quad (43)$$

$$[V] = [I(0) \ I(1) \ \dots \ I(m-1) \ I(m) \ J(0) \ J(1) \ \dots \ J(m-1) \ J(m) \ T(0) \ T(1) \ \dots \ T(n-1) \ T(n) \ L(0) \ L(1) \ \dots \ L(n-1) \ L(n)]^T \quad (44)$$

**Table 6**

The effect of material properties on the first five natural frequencies of a laminated cross-ply square CFRP composite plate slab with the stacking sequence of [0 90 0 90 90 0 90 0].

CFRP property	Method	Non-dimensional natural frequency: $\bar{\Psi}_j$				
		1	2	3	4	5
CFRP.1	Ritz [35]	15.76	48.72	58.25	67.64	74.65
	Present	15.45	48.37	57.52	67.55	74.24
CFRP.2	Ritz [35]	19.66	49.62	63.55	69.93	80.21
	Present	19.31	49.96	63.27	70.05	79.88
CFRP.3	Ritz [35]	15.89	49.71	59.23	70.17	77.06
	Present	15.59	50.12	59.15	70.29	76.85
CFRP.4	Ritz [35]	16.64	54.28	63.89	77.12	84.04
	Present	16.33	54.60	63.74	77.28	83.87
CFRP.5	Ritz [35]	16.62	51.82	61.79	72.93	80.18
	Present	16.29	51.81	61.34	72.93	79.85

In Eq. (43), the elements of the eigenfrequency matrix  $[\lambda]$ , labelled as  $\bar{S}_i$  and when  $i = \{3, 4, 7, 8, 9, 10, 13, 14\}$ , are computed by the following equations:

$$\bar{S}_3(n, \omega_j) = \sum_{m=0}^{\infty} S_3(m, n, \omega_j) \quad (45)$$

$$\bar{S}_4(n, \omega_j) = \sum_{m=0}^{\infty} S_4(m, n, \omega_j) \quad (46)$$

$$\bar{S}_7(n, \omega_j) = \sum_{m=0}^{\infty} S_7(m, n, \omega_j) \quad (47)$$

$$\bar{S}_8(n, \omega_j) = \sum_{m=0}^{\infty} S_8(m, n, \omega_j) \quad (48)$$

$$\bar{S}_9(m, \omega_j) = \sum_{n=0}^{\infty} S_9(m, n, \omega_j) \quad (49)$$

$$\bar{S}_{10}(m, \omega_j) = \sum_{n=0}^{\infty} S_{10}(m, n, \omega_j) \quad (50)$$

$$\bar{S}_{13}(m, \omega_j) = \sum_{n=0}^{\infty} S_{13}(m, n, \omega_j) \quad (51)$$

$$\bar{S}_{14}(m, \omega_j) = \sum_{n=0}^{\infty} S_{14}(m, n, \omega_j) \quad (52)$$

where, the elements of the eigenfrequency matrix  $([\lambda])$ , labelled as  $S_i$

**Table 7**

The combined effect of geometrical dimension and fiber angle orientation on the first five natural frequencies of the suspended laminated composite plate and with the constant thickness of  $H = 1.5$  (cm).

$\left(\frac{b}{a}\right)$	Method	Non-dimensional natural frequency: $\Psi_j$									
		[000]					[90 90 90]				
		1	2	3	4	5	1	2	3	4	5
1	Present	4.82	5.45	11.16	14.99	20.74	4.82	5.45	11.15	14.99	20.74
	FEM	4.89	5.46	11.36	15.02	21.11	4.89	5.46	11.36	15.02	21.11
	Error [%]	0.33	0.04	0.94	0.14	1.75	0.33	0.04	0.99	0.14	1.75
1.5	Present	2.42	3.17	6.68	6.88	11.70	13.25	22.25	34.65	40.49	48.14
	FEM	2.42	3.21	6.68	7.01	11.95	13.51	22.28	35.21	40.52	48.52
	Error [%]	0	0.08	0	0.26	0.51	0.53	0.06	1.15	0.06	0.78
2	Present	1.36	2.35	3.76	4.98	7.37	9.97	21.91	23.15	29.83	30.19
	FEM	1.36	2.39	3.76	5.06	7.37	10.17	21.94	23.16	30.20	30.54
	Error [%]	0	0.13	0	0.26	0	0.65	0.09	0.03	1.21	1.14
2.5	Present	0.12	0.27	0.36	0.58	0.70	7.96	14.55	21.59	22.32	27.29
	FEM	0.13	0.28	0.35	0.59	0.70	8.13	14.55	21.92	22.35	27.57
	Error [%]	0.03	0.03	0.03	0.03	0	0.61	0	1.19	0.1	1.01
3	Present	0.60	1.55	1.67	3.21	3.28	6.62	10.11	16.72	22.31	25.75
	FEM	0.60	1.57	1.67	3.25	3.28	6.75	10.11	17.01	22.33	25.94
	Error [%]	0	0.07	0	0.15	0	0.50	0	1.11	0.07	0.73
3.5	Present	0.44	1.23	1.33	2.41	2.72	6.62	10.11	16.72	22.31	25.75
	FEM	0.44	1.22	1.35	2.40	2.76	6.75	10.11	17.01	22.33	25.94
	Error [%]	0	0.03	0.07	0.03	0.15	0.50	0	1.11	0.07	0.73
4	Present	0.34	0.94	1.16	1.84	2.37	4.93	5.69	11.48	15.69	21.53
	FEM	0.34	0.94	1.17	1.84	2.40	5.02	5.69	11.72	15.68	21.91
	Error [%]	0	0	0.04	0	0.13	0.41	0	1.09	0.04	1.73
4.5	Present	0.26	0.74	1.03	1.45	2.09	4.36	4.49	9.93	12.40	18.05
	FEM	0.26	0.74	1.04	1.45	2.12	4.44	4.49	10.14	12.39	18.40
	Error [%]	0	0	0.05	0	0.16	0.43	0	1.14	0.05	1.90
5	Present	0.21	0.60	0.92	1.18	1.88	3.64	3.91	8.74	10.04	15.51
	FEM	0.21	0.60	0.94	1.18	1.90	3.64	3.99	8.93	10.04	15.83
	Error [%]	0	0	0.12	0	0.12	0	0.50	1.20	0	2.02

and when  $i = \{1, 2, 3, \dots, 16\}$ , are computed using the equations provided in Appendix B.

The determinant of an eigenfrequency matrix (Eq. (43)) must be equal to zero in order to acquire the natural frequencies and mode shapes of free vibration. To improve the accuracy of the analytical results and achieve convergence, the limited number of Fourier series terms,  $m = \{0, 1, 2, \dots, \infty\}$  and  $n = \{0, 1, 2, \dots, \infty\}$ , must be selected. Submission of the unknown terms  $I(m)$ ,  $J(m)$ ,  $T(n)$ , and  $L(n)$  into Eq. (31), and then Eq. (18) leads to the determination of the associated mode shapes in a suspended laminated composite slab.

An algorithm has been developed to capture the differences between the unacceptable and real natural frequencies through a filtering process as shown in Fig. 2. This algorithm can assist in distinguishing the discontinuity points and removing them from the eigenfrequency results.

In the present work, two non-dimensional natural frequencies are defined as:

$$\Psi_j = a^2 \omega_j \sqrt{\frac{\rho H}{D_{11}}} \quad (53)$$

$$\bar{\Psi}_j = \left( \frac{a^2 \omega_j}{H} \right) \sqrt{\frac{12\rho(1 - \nu_{12}\nu_{21})}{E_2}} \quad (54)$$

where,  $E_2$ ,  $\nu_{12}$ , and  $\nu_{21}$  are the elastic properties of a composite material [32].

Once the eigenfrequencies are obtained, they are substituted into the eigenfrequency matrix  $[\lambda]$ . This leads to the calculation of the eigenvector  $[V]$  containing the unknown terms  $I(m)$ ,  $J(m)$ ,  $T(n)$ , and  $L(n)$ . Finally, substituting the eigenfrequencies  $\omega_j$  and the obtained terms  $I(m)$ ,  $J(m)$ ,  $T(n)$ , and  $L(n)$  into Eq. (55) results in the calculation of the mode shapes of free transverse vibration:

$$\begin{aligned} W(x, y, \omega_j) = & \frac{1}{ab} [V_{11}(0, 0, \omega_j)I(0) + V_{12}(0, 0, \omega_j)J(0) + V_{13}(0, 0, \omega_j)T(0) + V_{14}(0, 0, \omega_j)L(0)] \\ & + \frac{2}{ab} \sum_{n=1}^{\infty} [V_{11}(0, n, \omega_j)I(0) + V_{12}(0, n, \omega_j)J(0) + V_{13}(0, n, \omega_j)T(n) + V_{14}(0, n, \omega_j)L(n)] \cos(\beta_n y) \\ & + \frac{2}{ab} \sum_{m=1}^{\infty} [V_{11}(m, 0, \omega_j)I(m) + V_{12}(m, 0, \omega_j)J(m) + V_{13}(m, 0, \omega_j)T(0) + V_{14}(m, 0, \omega_j)L(0)] \cos(\alpha_m x) \\ & + \frac{4}{ab} \sum_{m=1}^{\infty} \sum_{n=1}^{\infty} [V_{11}(m, n, \omega_j)I(m) + V_{12}(m, n, \omega_j)J(m) + V_{13}(m, n, \omega_j)T(n) + V_{14}(m, n, \omega_j)L(n)] \cos(\alpha_m x) \cos(\beta_n y) \end{aligned} \quad (55)$$

### 3. Validation and convergence studies

Comprehensive validation and convergence studies were conducted to explore the reliability and accuracy of the proposed analytical solution. The results of the solution procedure were first validated by the results available in the literature. The influence of convergence on the accuracy of analytical results was also explored. Due to a research gap in the literature, more complete and realistic case-study examples were then designed and verified by using the Finite Element (FE) package Abaqus. The analytical and numerical analyses considered the influence of transverse shear deformation, material anisotropy, rotary inertia, and the configuration of stacking sequence associated with composite lamination. The elastic properties of several materials used in the current study are provided in Table.1 and Table.2. In all cases associated with composite lamination, the ply thickness was kept constant, so that  $t_i = H \times k^{-1}$ , in which  $i$ ,  $t$ ,  $k$ , and  $H$  stand for the ply number, ply thickness, total number of plies, and total thickness of plate, respectively.

In the finite element modeling using Abaqus software in the present study, the C3D20R quadratic element was selected that represents a twenty-node quadratic brick with reduced integration. The C3D8R linear element with eight-nodes with reduced integration and hourglass control should not be chosen. This is because quadratic elements are more suitable to be utilized for complex geometries and bending deformations within static and dynamic domains. This is a main disadvantage of using FEM for vibration analysis of relatively large plates since a quadratic element is computationally expensive and larger plates contain more elements and nodal connections. A careful mesh convergence study was conducted for the numerical modeling to ensure the results convergence/sensitivity and accuracy. The optimum mesh number significantly varies case by case. In Abaqus, the procedure type for frequency response analysis was selected to be the linear perturbation within the step module.

The eigenfrequencies of a suspended aluminum square slab possessing various Poisson's ratios were first studied using the present analytical method and then compared with the results of the references [15,16]. Indeed, it is a special case-study in which the effect of material anisotropy, lamination sequence, transverse shear deformation, and rotary inertia were all ignored. Nevertheless, it could be used as a benchmark to verify the proposed analytical solution. The results in the literature were calculated using Hamiltonian system-based analytical modeling (HMN), FEM, and analytical modeling. The comparison of results obtained is provided in Table 3. It can be seen from Table 3 that the analytical results are well within the acceptable range of the results obtained from other methods.

The use of the proposed root-finding algorithm to calculate the eigenfrequencies of plates in Table 3 is illustrated in Fig. 3. The convergence study also demonstrates that the analytical solution can easily converge with small series terms, leading to accurate results. The results from all approaches demonstrate that an increase in the Poisson's

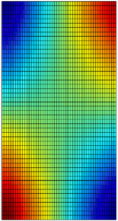
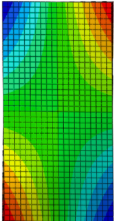
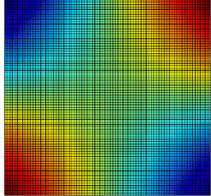
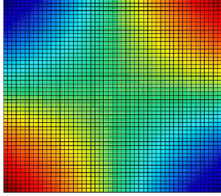
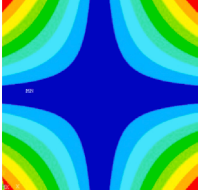
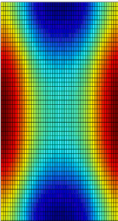
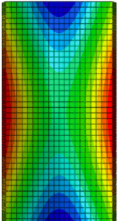
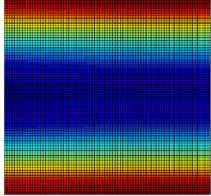
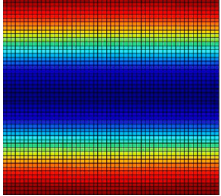
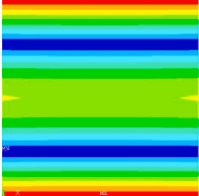
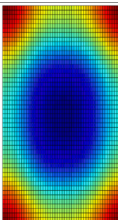
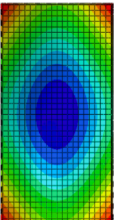
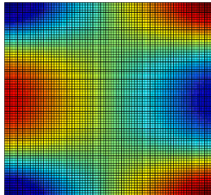
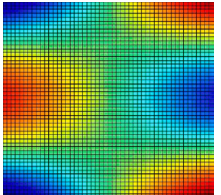
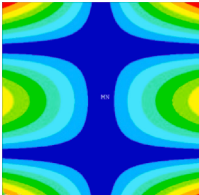
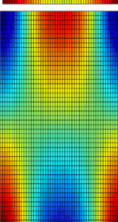
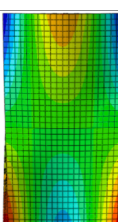
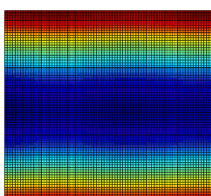
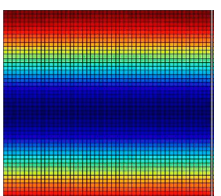
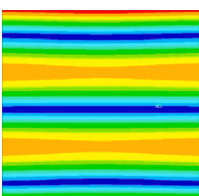
ratio of a material with a same elastic modulus and density results in a decrease in the natural frequencies of free vibration.

The effect of geometrical dimension such as aspect ratio ( $R = b \times a^{-1}$ ) on the eigenfrequencies of several suspended rectangular plate structures made of aluminum was further explored and compared with the reference [16], which are based on HMN and FEM. The comparison of the results is tabulated in Table.4, which shows good agreement when considering the first ten dimensionless natural frequencies. It is observed that the natural frequencies decrease as  $R$  increases regardless of the mode number. This is because higher  $R$  value results in more mass, thereby lowering the frequency response.

The eigenfrequencies of the suspended plate slab made of a composite material were determined, considering various geometrical dimensions. The results obtained are compared with the analytical and FEM results available in references [33,34] in Table 5. The application of the proposed root finding algorithm for the composite case is demonstrated in Fig. 4. The proposed analysis solution predicts well the first ten natural frequencies, thereby demonstrating its reliability and

**Table 8**

The mode shapes of several suspended laminated composite slabs.

T300/976 CFRP, $R = 2$ , $H = 5$ cm, [90/90/90/90/90]		$R = 1$ , $(H/b) = 0.2$ , $(E_{11}/E_{22}) = 40$ , $G_{12} = G_{13} = (3/5)E_{22}$ , $G_{23} = (1/2)E_{22}$ , $\nu_{12} = \nu_{13} = \nu_{23} = 0.3$ , [0/90/0]		
Present study	FEM	Present study	Analytical [36]	FEM [36]
				
				
				
				

accuracy. It can be observed from Table.5 that increasing the  $R$  ratio in a plate decreases the natural frequencies, regardless of material anisotropy.

The effect of material properties on the first five natural frequencies of a suspended laminated cross-ply square composite plate was studied. It was assumed that the plate was made of CFRP composites with various elastic properties. The results of the proposed analytical solution are compared with the results given in reference [35], which was an analytical solution based on the Ritz Theory. Table.6 shows that the agreement between two analytical solutions is good. The elastic property variation within a same composite material demonstrates to have an insignificant impact on the eigenfrequencies of free vibration.

The combined effect of the plate's aspect ratio and fiber angle orientation  $\beta$  on the first five natural frequencies of the suspended laminated rectangular composite slabs was explored through the proposed analytical method and FEM. It is seen from Table.7 that there is a good agreement between the proposed analytical solution and FEM developed using Abaqus with the relative error of less than 2% for all cases. As per Table.7, two types of three-layered composite slabs were selected with different fiber angle orientation ([0/0/0] and [90/90/90]). The plates were made of T300/976 CFRP (see Table.1). It can be observed that the fiber angle orientation of the plates can significantly influence the free vibration response irrespective of the variation of  $R$  ratio. For example, the natural frequency of the plate with  $\beta = 90^\circ$  is higher than that of the one with  $\beta = 0^\circ$ .

The first four exact mode shapes of a suspended laminated rectangular composite slab were investigated using the present analytical solution and FEM. Two types of laminated cross-ply composite plate slabs were selected, which differed in the geometry, elastic properties, and number of layers. The reliability of the proposed analytical solution was evaluated by comparing with FEM and the results of reference [36]. Table.8 demonstrates that the proposed solution procedure accurately predicts the mode shapes of vibration. The proposed method can be used to explore the eigenfrequencies within a higher range of spectrum since no mesh sensitivity analysis and changes of parametric variables are required unlike FEM.

Table.9 shows the effect of lamination sequence on the frequency response of the suspended laminated rectangular slabs. The first five natural frequencies for each lamination case were calculated using the proposed analytical solution and FEM. The proposed analytical solution agrees well with the results obtained by the FEM with the relative error of less than 2% for all cases. The results clearly show that stacking sequence alone can significantly influence the eigenfrequencies. As such, a proper selection of lamination can potentially be beneficial in altering the vibration response of suspended slabs to avoid frequency resonance in the area susceptible to high seismic activities.

Another critical factor affecting the free vibration response of plates is the material property. To investigate the sole effect of material property on the fundamental natural frequency of a suspended one-layered square plate, four materials were selected from Table 1. The

**Table 9**

The effect of stacking sequence on the first five natural frequencies of the suspended laminated composite rectangular slab ( $R = 2$ ) made of T300/976 CFRP and with the constant total thickness of  $H = 5$  (cm).

Lamination sequence	Method	Non-dimensional natural frequency: $\Psi_j$				
		1	2	3	4	5
[0/90/0/90/0]	Present	2.64	3.12	6.16	8.49	11.46
	FEM	2.69	3.12	6.27	8.47	11.64
	Error [%]	0.42	0	0.94	0.17	1.54
[90/0/90/0/90]	Present	4.76	9.76	13.52	21.66	23.44
	FEM	4.85	9.78	13.72	21.76	23.63
	Error [%]	0.38	0.08	0.84	0.42	0.80
[0/0/90/0/0]	Present	1.44	2.32	3.96	4.91	7.68
	FEM	1.45	2.36	3.98	5.00	7.76
	Error [%]	0.12	0.51	0.25	1.15	1.03
[90/90/0/90/90]	Present	9.23	20.82	22.09	27.69	28.20
	FEM	9.40	20.90	22.35	28.05	28.78
	Error [%]	0.59	0.27	0.90	1.25	2.01
[0/0/0/0/0]	Present	1.35	2.30	3.71	4.84	7.18
	FEM	1.36	2.34	3.73	4.94	7.27
	Error [%]	0.13	0.55	0.27	1.37	1.23
[90/90/90/90/90]	Present	9.79	21.49	22.79	28.87	29.45
	FEM	9.99	21.74	22.96	29.57	29.95
	Error [%]	0.66	0.83	0.56	2.33	1.66

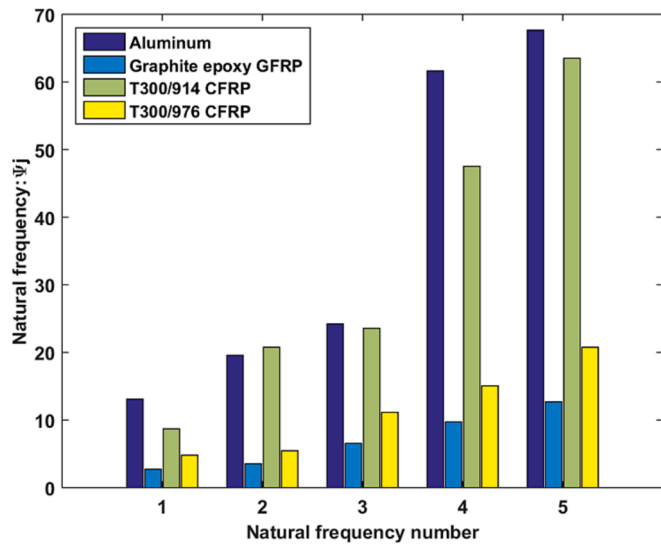


**Fig. 5.** The influence of material properties on the first five natural frequencies response of a suspended one-layered composite square plate slab with the constant total thickness of  $H = 5$  (cm).

aspect ratio, thickness and fiber orientations were kept constant in all cases. When the plates were made of composite material, the fiber angle orientation was kept at  $\beta = 0^\circ$ . The results are illustrated in Fig. 5. Like several factors affecting free vibration as discussed before, the elastic properties of a suspended slab also have a considerable effect on the free vibration response.

Fig. 6 shows the effect of the thickness of plate on the fundamental natural frequency of suspended slabs possessing isotropic and anisotropic properties. The results against diverse range of aspect ratios  $R$  were explored. The analytical results demonstrate that increasing the thickness reduces the natural frequency of vibration regardless of the

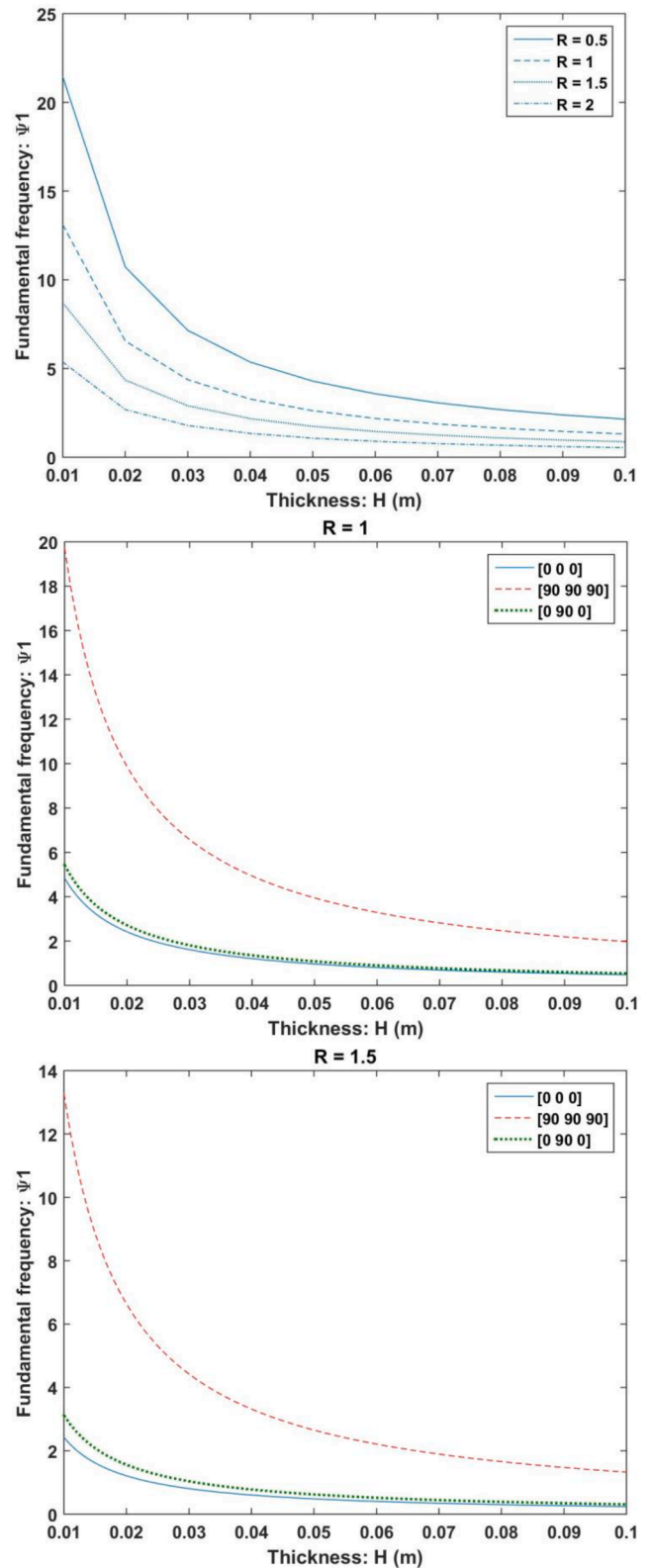


**Fig. 6.** The influence of thickness on the non-dimensional fundamental natural frequency in the suspended isotropic and laminated composite plate slabs of various.

geometrical dimensions and material property. It is observed that the changes of frequency versus thickness have a nonlinear trend. When increasing the thickness to a certain level, the change in the frequency response becomes marginal and negligible. Furthermore, for a specific

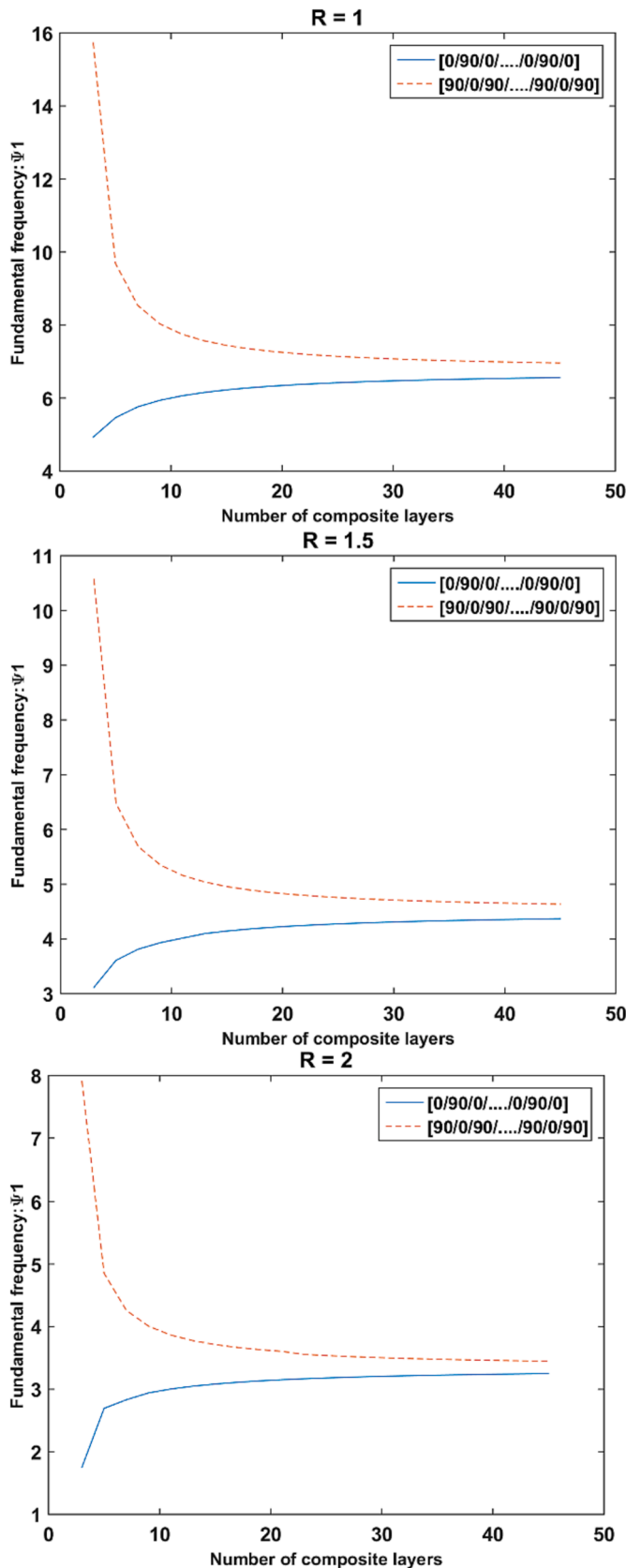


Fig. 7. The combined effect of layer number and fiber angle on fundamental frequency response of various suspended laminated composite plate slabs with the constant total thickness of  $H = 5$  (cm).

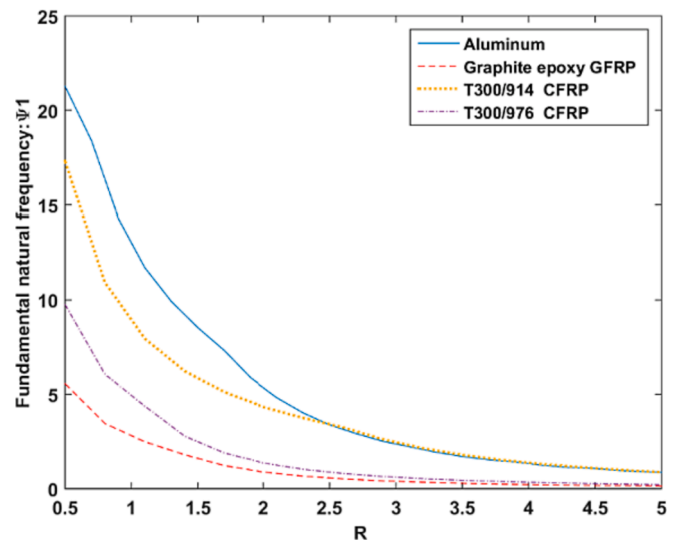


Fig. 8. The combined effect of  $R$  ratio and material properties on the fundamental natural frequency of vibration in the suspended laminated composite plate slab with the total constant thickness of  $H = 1$  (cm).

type of material, an increase in the  $R$  ratio leads to lower frequency response.

The effect of the number of composite layers on free vibration response of suspended laminated composite plates of various sizes was studied. The total thickness  $H$  and material properties were kept constant to explore the pure effect of ply number on the fundamental natural frequency. Two types of stacking sequence configuration were chosen including  $[0/90/0/.../0/90/0]$  and  $[90/0/90/.../90/0/90]$  and the frequency changes within the diverse range of  $k = [3-45]$  were examined. The analytical results, which are shown in Fig. 7, demonstrate that there is a sharp decline and increase in the frequency responses up to approximately 10 layers for  $[90/0/90/.../90/0/90]$  and  $[0/90/0/.../0/90/0]$ , respectively. These changes become insignificant when more than 10 layers are sought regardless of the arrangement of stacking sequence, according to Fig. 7.

In the final case-study as shown in Fig. 8, both the effect of material properties and the aspect ratio ( $R$ ) of a plate on the fundamental frequency of various one-layered suspended composite slabs were examined. The total thickness of the plates was kept constant. When the plates were made of composite material, the number of layers and fiber angles were kept at  $k = 1$  and  $\beta = 0^\circ$ , respectively. According to Fig. 7, increasing the aspect ratio  $R$  leads to a sharp decline in the magnitude of the fundamental frequency regardless of the changes in the elastic properties of the plates. However, such a significant decrease is observed within a finite range of  $R = [0.5-2.5]$ . These changes in the frequency response become negligible and small from  $R = [2.5-5]$  and are expected to continue the same trend for the aspect ratios larger than  $R = 5$ . Overall, the change in the frequency versus the aspect ratio of the plate is nonlinear.

#### 4. Conclusions

A complete analytical solution to the dynamic response of suspended laminated composite slabs has been developed and described in this paper. In the analytical method, the theory of elasticity is utilized to establish the equations of motion which are solved using higher-order trigonometric series. The developed method accounts for the effect of transverse shear, material anisotropy, lamination, and rotatory inertia. It has the capability of calculating the eigenfrequencies and mode shapes of vibration regardless of the degree of material anisotropy, thickness of plates, in-plane geometrical dimension of plates, and the number of layers.

The followings concluding remarks are provided:

- The proposed analytical solution has been verified by comparisons with existing solutions and the finite element results of Abaqus package.
- The mathematical derivation of the analytical method is rigorous without the prior consideration of the flexural deformation and separate-of-variable forms, leading to more accurate results compared to other solution procedures such as FEM.
- The formulated analytical method is computationally more efficient than the FEM since it converges quickly and doesn't require any mesh sensitivity analysis.
- The developed solution procedure is efficient in exploring the variety of problems since the theoretical formulation and the simulation codes during the parametric studies do not need to be altered unlike the FEM.
- The significant effect of critical factors highlights a need for a more complex solution procedure dealing with the broad range of free vibration problems associated with suspended slabs.
- The solution procedure designed is only applicable to the transverse vibration response of suspended plate slabs and cannot be used for plates with other boundary conditions.
- Since an earthquake can generate the thickness shear, twist and stretch, and in-plane vibrations, further study should be conducted to

calculate the eigenfrequencies and mode shapes associated with other types of vibration responses.

**CRedit authorship contribution statement**

**Soheil Gohari:** Conceptualization, Methodology, Software, Validation, Formal analysis, Investigation, Data curation, Writing – original draft, Visualization, Project administration. **Mizan Ahmed:** Visualization, Project administration, Writing – review & editing. **Qing Quan Liang:** Visualization, Project administration, Writing – review & editing. **Tesfaye Molla:** Conceptualization, Methodology, Visualization, Writing – review & editing. **Mladenko Kajtaz:** Conceptualization, Methodology, Visualization, Writing – review & editing. **Kwong Ming Tse:** Conceptualization, Methodology, Visualization, Writing – review & editing. **Colin Burvill:** Writing – review & editing.

**Declaration of Competing Interest**

The authors declare that they have no known competing financial interests or personal relationships that could have appeared to influence the work reported in this paper.

**Data availability**

Data will be made available on request.

**Appendix A**

The elements of the constitutive dynamic matrix in Eq.31 are calculated as follows:

$$\begin{aligned}
 V_{11}(m, n, \omega_j) &= \left\{ \left[ \frac{\Omega_2(m, n, \omega_j)\Omega_3(m, n, \omega_j) - \Omega_1(m, n, \omega_j)\Omega_4(m, n, \omega_j)}{\Omega_3(m, n, \omega_j)} \right] \right. \\
 &\times \left. \left[ \frac{\Omega_3(m, n, \omega_j)\Omega_{11}(m, n) - \Omega_5(m, n)\Omega_9(m, n, \omega_j)}{\Omega_3(m, n, \omega_j)\Omega_{10}(m, n, \omega_j) - \Omega_4(m, n, \omega_j)\Omega_9(m, n, \omega_j)} \right] \right\} + \left[ \frac{\Omega_1(m, n, \omega_j)\Omega_5(m, n)}{\Omega_3(m, n, \omega_j)} \right] \\
 V_{12}(m, n, \omega_j) &= \left\{ \left[ \frac{\Omega_2(m, n, \omega_j)\Omega_3(m, n, \omega_j) - \Omega_1(m, n, \omega_j)\Omega_4(m, n, \omega_j)}{\Omega_3(m, n, \omega_j)} \right] \right. \\
 &\times \left. \left[ \frac{\Omega_3(m, n, \omega_j)\Omega_{12}(m, n) - \Omega_6(m, n)\Omega_9(m, n, \omega_j)}{\Omega_3(m, n, \omega_j)\Omega_{10}(m, n, \omega_j) - \Omega_4(m, n, \omega_j)\Omega_9(m, n, \omega_j)} \right] \right\} + \left[ \frac{\Omega_1(m, n, \omega_j)\Omega_6(m, n)}{\Omega_3(m, n, \omega_j)} \right] \\
 V_{13}(m, n, \omega_j) &= \left\{ \left[ \frac{\Omega_2(m, n, \omega_j)\Omega_3(m, n, \omega_j) - \Omega_1(m, n, \omega_j)\Omega_4(m, n, \omega_j)}{\Omega_3(m, n, \omega_j)} \right] \right. \\
 &\times \left. \left[ \frac{\Omega_3(m, n, \omega_j)\Omega_{13}(m, n) - \Omega_7(m, n)\Omega_9(m, n, \omega_j)}{\Omega_3(m, n, \omega_j)\Omega_{10}(m, n, \omega_j) - \Omega_4(m, n, \omega_j)\Omega_9(m, n, \omega_j)} \right] \right\} + \left[ \frac{\Omega_1(m, n, \omega_j)\Omega_7(m, n)}{\Omega_3(m, n, \omega_j)} \right] \\
 V_{14}(m, n, \omega_j) &= \left\{ \left[ \frac{\Omega_2(m, n, \omega_j)\Omega_3(m, n, \omega_j) - \Omega_1(m, n, \omega_j)\Omega_4(m, n, \omega_j)}{\Omega_3(m, n, \omega_j)} \right] \right. \\
 &\times \left. \left[ \frac{\Omega_3(m, n, \omega_j)\Omega_{14}(m, n) - \Omega_8(m, n)\Omega_9(m, n, \omega_j)}{\Omega_3(m, n, \omega_j)\Omega_{10}(m, n, \omega_j) - \Omega_4(m, n, \omega_j)\Omega_9(m, n, \omega_j)} \right] \right\} + \left[ \frac{\Omega_1(m, n, \omega_j)\Omega_8(m, n)}{\Omega_3(m, n, \omega_j)} \right] \\
 V_{21}(m, n, \omega_j) &= \left[ \frac{\Omega_5(m, n)}{\Omega_3(m, n, \omega_j)} \right] - \left\{ \left[ \frac{\Omega_4(m, n, \omega_j)}{\Omega_3(m, n, \omega_j)} \right] \left[ \frac{\Omega_3(m, n, \omega_j)\Omega_{11}(m, n) - \Omega_5(m, n)\Omega_9(m, n, \omega_j)}{\Omega_3(m, n, \omega_j)\Omega_{10}(m, n, \omega_j) - \Omega_4(m, n, \omega_j)\Omega_9(m, n, \omega_j)} \right] \right\} \\
 V_{22}(m, n, \omega_j) &= \left[ \frac{\Omega_6(m, n)}{\Omega_3(m, n, \omega_j)} \right] - \left\{ \left[ \frac{\Omega_4(m, n, \omega_j)}{\Omega_3(m, n, \omega_j)} \right] \left[ \frac{\Omega_3(m, n, \omega_j)\Omega_{12}(m, n) - \Omega_6(m, n)\Omega_9(m, n, \omega_j)}{\Omega_3(m, n, \omega_j)\Omega_{10}(m, n, \omega_j) - \Omega_4(m, n, \omega_j)\Omega_9(m, n, \omega_j)} \right] \right\} \\
 V_{23}(m, n, \omega_j) &= \left[ \frac{\Omega_7(m, n)}{\Omega_3(m, n, \omega_j)} \right] - \left\{ \left[ \frac{\Omega_4(m, n, \omega_j)}{\Omega_3(m, n, \omega_j)} \right] \left[ \frac{\Omega_3(m, n, \omega_j)\Omega_{13}(m, n) - \Omega_7(m, n)\Omega_9(m, n, \omega_j)}{\Omega_3(m, n, \omega_j)\Omega_{10}(m, n, \omega_j) - \Omega_4(m, n, \omega_j)\Omega_9(m, n, \omega_j)} \right] \right\}
 \end{aligned}$$

$$V_{24}(m, n, \omega_j) = \frac{\Omega_8(m, n)}{\Omega_3(m, n, \omega_j)} - \left\{ \left[ \frac{\Omega_4(m, n, \omega_j)}{\Omega_3(m, n, \omega_j)} \right] \left[ \frac{\Omega_3(m, n, \omega_j)\Omega_{14}(m, n) - \Omega_8(m, n)\Omega_9(m, n, \omega_j)}{\Omega_3(m, n, \omega_j)\Omega_{10}(m, n, \omega_j) - \Omega_4(m, n, \omega_j)\Omega_9(m, n, \omega_j)} \right] \right\}$$

$$V_{31}(m, n, \omega_j) = \frac{\Omega_3(m, n, \omega_j)\Omega_{11}(m, n) - \Omega_5(m, n)\Omega_9(m, n, \omega_j)}{\Omega_3(m, n, \omega_j)\Omega_{10}(m, n, \omega_j) - \Omega_4(m, n, \omega_j)\Omega_9(m, n, \omega_j)}$$

$$V_{32}(m, n, \omega_j) = \frac{\Omega_3(m, n, \omega_j)\Omega_{12}(m, n) - \Omega_6(m, n)\Omega_9(m, n, \omega_j)}{\Omega_3(m, n, \omega_j)\Omega_{10}(m, n, \omega_j) - \Omega_4(m, n, \omega_j)\Omega_9(m, n, \omega_j)}$$

$$V_{33}(m, n, \omega_j) = \frac{\Omega_3(m, n, \omega_j)\Omega_{13}(m, n) - \Omega_7(m, n)\Omega_9(m, n, \omega_j)}{\Omega_3(m, n, \omega_j)\Omega_{10}(m, n, \omega_j) - \Omega_4(m, n, \omega_j)\Omega_9(m, n, \omega_j)}$$

$$V_{34}(m, n, \omega_j) = \frac{\Omega_3(m, n, \omega_j)\Omega_{14}(m, n) - \Omega_8(m, n)\Omega_9(m, n, \omega_j)}{\Omega_3(m, n, \omega_j)\Omega_{10}(m, n, \omega_j) - \Omega_4(m, n, \omega_j)\Omega_9(m, n, \omega_j)}$$

where, the coefficients  $\Omega_1, \Omega_2, \dots, \Omega_{13}$ , and  $\Omega_{14}$  are calculated as follows:

$$\Omega_1(m, n, \omega_j) = \zeta_1(m, n, \omega_j)$$

$$\Omega_2(m, n, \omega_j) = \zeta_2(m, n, \omega_j)$$

$$\Omega_3(m, n, \omega_j) = (D_{11}\alpha_m^2 + D_{66}\beta_n^2 + K_s A_{55} - \rho_2 \omega_j^2) - K_s A_{55} \alpha_m \zeta_1(m, n, \omega_j)$$

$$\Omega_4(m, n, \omega_j) = (D_{12} + D_{66})\alpha_m \beta_n - K_s A_{55} \alpha_m \zeta_2(m, n, \omega_j)$$

$$\Omega_5(m, n) = -D_{12} \alpha_m (-1)^n$$

$$\Omega_6(m, n) = D_{12} \alpha_m J(m)$$

$$\Omega_7(m, n) = -D_{11} \alpha_m (-1)^m$$

$$\Omega_8(m, n) = D_{11} \alpha_m$$

$$\Omega_9(m, n, \omega_j) = (D_{12} + D_{66})\alpha_m \beta_n - K_s A_{44} \beta_n \zeta_1(m, n, \omega_j)$$

$$\Omega_{10}(m, n, \omega_j) = (D_{66}\alpha_m^2 + D_{22}\beta_n^2 + K_s A_{44} - \rho_2 \omega_j^2) - K_s A_{44} \beta_n \zeta_2(m, n, \omega_j)$$

$$\Omega_{11}(m, n) = -D_{22} \beta_n (-1)^n$$

$$\Omega_{12}(m, n) = D_{22} \beta_n$$

$$\Omega_{13}(m, n) = -D_{12} (-1)^m$$

$$\Omega_{14}(m, n) = D_{12} \beta_n$$

**Appendix B**

The elements of the eigenfrequency matrix ( $[\lambda]$ ), labelled as  $S_i$  when  $i = \{1, 2, 3, \dots, 16\}$ , can be computed using the equations provided as follows:

$$S_1(m, n, \omega_j) = \Delta_m \Delta_n [D_{12}(-1)^n + D_{11} \alpha_m V_{21}(m, n, \omega_j) + D_{12} \beta_n V_{31}(m, n, \omega_j)]$$

$$S_2(m, n, \omega_j) = \Delta_m \Delta_n [D_{11} \alpha_m V_{22}(m, n, \omega_j) + D_{12} \beta_n V_{32}(m, n, \omega_j) - D_{12}]$$

$$S_3(m, n, \omega_j) = \Delta_m \Delta_n [D_{11}(-1)^m + D_{11} \alpha_m V_{23}(m, n, \omega_j) + D_{12} \beta_n V_{33}(m, n, \omega_j)]$$

$$S_4(m, n, \omega_j) = \Delta_m \Delta_n [D_{11} \alpha_m V_{24}(m, n, \omega_j) + D_{12} \beta_n V_{34}(m, n, \omega_j) - D_{11}]$$

$$S_5(m, n, \omega_j) = \Delta_m \Delta_n [D_{12}(-1)^m (-1)^n + D_{11} \alpha_m (-1)^m V_{21}(m, n, \omega_j) + D_{12} \beta_n (-1)^m V_{31}(m, n, \omega_j)]$$

$$S_6(m, n, \omega_j) = \Delta_m \Delta_n [D_{11} \alpha_m (-1)^m V_{22}(m, n, \omega_j) + D_{12} \beta_n (-1)^m V_{32}(m, n, \omega_j) - D_{12}(-1)^m]$$

$$S_7(m, n, \omega_j) = \Delta_m \Delta_n [D_{11}(-1)^{2m} + D_{11} \alpha_m (-1)^m V_{23}(m, n, \omega_j) + D_{12} \beta_n (-1)^m V_{33}(m, n, \omega_j)]$$

$$S_8(m, n, \omega_j) = \Delta_m \Delta_n [D_{11} \alpha_m (-1)^m V_{24}(m, n, \omega_j) + D_{12} \beta_n (-1)^m V_{34}(m, n, \omega_j) - D_{11}(-1)^m]$$

$$S_9(m, n, \omega_j) = \Delta_m \Delta_n [D_{22}(-1)^n + D_{12} \alpha_m V_{21}(m, n, \omega_j) + D_{22} \beta_n V_{31}(m, n, \omega_j)]$$

$$S_{10}(m, n, \omega_j) = \Delta_m \Delta_n [D_{12} \alpha_m V_{22}(m, n, \omega_j) + D_{22} \beta_n V_{32}(m, n, \omega_j) - D_{22}]$$

$$S_{11}(m, n, \omega_j) = \Delta_m \Delta_n [D_{12}(-1)^m + D_{12} \alpha_m V_{23}(m, n, \omega_j) + D_{22} \beta_n V_{33}(m, n, \omega_j)]$$

$$S_{12}(m, n, \omega_j) = \Delta_m \Delta_n [D_{12} \alpha_m V_{24}(m, n, \omega_j) + D_{22} \beta_n V_{34}(m, n, \omega_j) - D_{12}]$$

$$S_{13}(m, n, \omega_j) = \Delta_m \Delta_n [D_{22}(-1)^{2n} + D_{12} \alpha_m (-1)^n V_{21}(m, n, \omega_j) + D_{22} \beta_n (-1)^n V_{31}(m, n, \omega_j)]$$

$$S_{14}(m, n, \omega_j) = \Delta_m \Delta_n [D_{12} \alpha_m (-1)^n V_{22}(m, n, \omega_j) + D_{22} \beta_n (-1)^n V_{32}(m, n, \omega_j) - D_{22}(-1)^n]$$

$$S_{15}(m, n, \omega_j) = \Delta_m \Delta_n [D_{12}(-1)^m (-1)^n + D_{12} \alpha_m (-1)^n V_{23}(m, n, \omega_j) + D_{22} \beta_n (-1)^n V_{33}(m, n, \omega_j)]$$

$$S_{16}(m, n, \omega_j) = \Delta_m \Delta_n [D_{12} \alpha_m (-1)^n V_{24}(m, n, \omega_j) + D_{22} \beta_n (-1)^n V_{34}(m, n, \omega_j) - D_{12}(-1)^n]$$

## References

- [1] Mishra BB, Kumar A, Topal U. Stochastic normal mode frequency analysis of hybrid angle ply laminated composite skew plate with opening using a novel approach. *Mech Based Des Struct Mach Jan.* 2023;51(1):275–309.
- [2] Kumar A, Chakrabarti A, Bhargava P. Vibration analysis of laminated composite skew cylindrical shells using higher order shear deformation theory. *J Vib Control Mar.* 2015;21(4):725–35.
- [3] Chaubey AK, Kumar A, Mishra SS. Dynamic analysis of laminated composite rhombic elliptical paraboloid due to mass variation. *J Aerosp Eng* 2018;31(5):Sep.
- [4] Chaubey AK, Kumar A, Chakrabarti A. Vibration of laminated composite shells with cutouts and concentrated mass. *AIAA J Apr.* 2018;56(4):1662–78.
- [5] Qiu Z, Fan H. Laminated bamboo materials for plated building structures. *J Build Eng* 61(September); Dec. 2022:105239.
- [6] Choi K-K, Kim J-C. Nonlinear model simulating load–deformation relationship of flat plate structures. *Eng Struct Feb.* 2015;85:26–35.
- [7] Tatemichi I, Kawaguchi M, Abe M. A study on pendulum seismic isolators for high-rise buildings. In: CTBUH 2004 Seoul 2009;no. 056:p. n/a-n/a.
- [8] “Isolating a floor/ceiling – a real case,” *Ultrafonic*; 2019. <https://www.ultrafonic.com.au/blog/2019/10/21/isolating-a-floorceiling-a-real-case>.
- [9] “Architecture and Design,” Rondo KEY-LOCK® concealed suspended ceiling system. <https://www.architectureanddesign.com.au/suppliers/rondo/ceiling-systems>.
- [10] Feng MQ, Mita A. Vibration control of tall buildings using mega subconfiguration. *J Eng Mech Oct.* 1995;121(10):1082–8.
- [11] Lin C-C, Lin G-L, Wang J-F. Protection of seismic structures using semi-active friction TMD. *Earthq Eng Struct Dyn* 2009;no. 056:p. n/a-n/a.
- [12] Nagarajaiah S, Sonmez E. Structures with semiactive variable stiffness single/multiple tuned mass dampers. *J Struct Eng Jan.* 2007;133(1):67–77.
- [13] Ramallo JC, Johnson EA, Spencer BF. ‘Smart’ base isolation systems. *J Eng Mech Oct.* 2002;128(10):1088–99.
- [14] Mahmoud H, Chulawahat A. Response of building systems with suspended floor slabs under dynamic excitations. *Eng Struct Dec.* 2015;104(27235):155–73.
- [15] Leissa AW. NASA SP-160, Office of technology utilization, vibration of plates. Washington DC; 1969.
- [16] Li R, Wang B, Li G, Tian B. Hamiltonian system-based analytic modeling of the free rectangular thin plates’ free vibration. *App Math Model Jan.* 2016;40(2):984–92.
- [17] Zhong Y, Zhao X, Liu H. Vibration of plate on foundation with four edges free by finite cosine integral transform method. *Lat Am J Solids Struct Oct.* 2014;11(5):854–63.
- [18] Hu Z, et al. Symplectic superposition solutions for free in-plane vibration of orthotropic rectangular plates with general boundary conditions. *Sci Rep Feb.* 2023;13(1):2601.
- [19] Dozio L. In-plane free vibrations of single-layer and symmetrically laminated rectangular composite plates. *Compos Struct Jun.* 2011;93(7):1787–800.
- [20] Wang Z, Xing Y, Sun Q. Highly accurate closed-form solutions for the free in-plane vibration of rectangular plates with arbitrary homogeneous boundary conditions. *J Sound Vib Mar.* 2020;470:115166.
- [21] Du J, Li WL, Jin G, Yang T, Liu Z. An analytical method for the in-plane vibration analysis of rectangular plates with elastically restrained edges. *J Sound Vib Oct.* 2007;306(3–5):908–27.
- [22] Bardell NS, Langley RS, Dunsdon JM. On the free in-plane vibration of isotropic rectangular plates. *J Sound Vib Apr.* 1996;191(3):459–67.
- [23] Zhang Y, Du J, Yang T, Liu Z. A series solution for the in-plane vibration analysis of orthotropic rectangular plates with elastically restrained edges. *Int J Mech Sci Feb.* 2014;79:15–24.
- [24] Vinson JR. Plate and panel structures of isotropic, composite and piezoelectric materials, including sandwich construction, vol. 120. Dordrecht: Springer, Netherlands; 2005.
- [25] Reddy JN. On laminated composite plates with integrated sensors and actuators. *Eng Struct Jul.* 1999;21(7):568–93.
- [26] Gohari S, et al. A new analytical solution for elastic flexure of thick multi-layered composite hybrid plates resting on Winkler elastic foundation in air and water. *Ocean Eng* 235(July);Sep. 2021:109372.
- [27] Y. Wang, H. Ren, T. Fu, and C. Shi, “Hygrothermal mechanical behaviors of axially functionally graded microbeams using a refined first order shear deformation theory,” *Acta Astronaut.*, vol. 166, no. October 2019, pp. 306–316, Jan. 2020.
- [28] Cornacchia F, Fantuzzi N, Luciano R, Penna R. Solution for cross- and angle-ply laminated Kirchhoff nano plates in bending using strain gradient theory. *Compos B Eng* 2019;173:107006.
- [29] Gohari S, et al. Static and dynamic deformation response of smart laminated composite plates induced by inclined piezoelectric actuators. *J Compos Mater Sep.* 2022;56(21):3269–93.
- [30] Akavci SS. Analysis of thick laminated composite plates on an elastic foundation with the use of various plate theories. *Mech Compos Mater Sep.* 2005;41(5):445–60.
- [31] Gohari S, et al. On 3D exact free torsional-bending vibration and buckling of biaxially loaded isotropic and anisotropic Timoshenko beams with complex cross-section. *Structures Mar.* 2023;49:1044–77.
- [32] Gohari S, Sharifi S, Vrcelj Z, Yahya MY. First-ply failure prediction of an unsymmetrical laminated ellipsoidal woven GFRP composite shell with incorporated surface-bounded sensors and internally pressurized. *Compos B Eng Aug.* 2015;77:502–18.
- [33] Li R, et al. New analytic free vibration solutions of orthotropic rectangular plates by a novel symplectic approach. *Acta Mechanica Sep.* 2019;230(9):3087–101.
- [34] Su X, Bai E. Analytical free vibration solutions of fully free orthotropic rectangular thin plates on two-parameter elastic foundations by the symplectic superposition method. *J Vib Control Jan.* 2022;28(1–2):3–16.
- [35] Narita Y, Innami N. Natural frequencies of laminated CFRP square plates with slightly different material properties. *IOP Conf Ser Mater Sci Eng Nov.* 2019;676(1):012027.
- [36] Xue Z, Li Q, Huang W, Guo Y, Wang J. Vibration characteristics analysis of moderately thick laminated composite plates with arbitrary boundary conditions. *Materials (Basel) Sep.* 2019;12(17):2829.
- [37] Wang D, et al. The influence of geometric imperfections on post-buckling behavior and free vibrations of a fiber-reinforced composite laminated plate under thermal loading. *Compos Struct* 306(November 2021); Feb. 2023:116568.
- [38] Vescovini R, Dozio L. Thermal buckling behaviour of thin and thick variable-stiffness panels. *J Compos Sci Oct.* 2018;2(4):58.
- [39] Peng X, Zhong Y, Shi J, Shi Z. Free flexural vibration analysis of composite sandwich plate with reentrant honeycomb cores using homogenized plate model. *J Sound Vib* 529(December 2021);2022:1–22.
- [40] Gohari S, Sharifi S, Vrcelj Z. New explicit solution for static shape control of smart laminated cantilever piezo-composite-hybrid plates/beams under thermo-electro-mechanical loads using piezoelectric actuators. *Compos Struct Jun.* 2016;145:89–112.
- [41] Tamijani AY, Abouhamze M, Mirzaeifar R, Ohadi AR, Eslami MR. Feedback control of piezo-laminate composite plate. In: 14th International Congress on sounds and Vibration, Cairns Australia, 9-12 July, 2007.
- [42] Yu Y, Zhang XN, Xie SL. Optimal shape control of a beam using piezoelectric actuators with low control voltage. *Smart Mater Struct Sep.* 2009;18(9):095006.
- [43] Stanford BK, Jutte CV. Comparison of curvilinear stiffeners and tow steered composites for aeroelastic tailoring of aircraft wings. *Comput Struct Apr.* 2017;183:48–60.
- [44] Vinson JR, Sierakowski RL. The behavior of structures composed of composite materials, vol. 105. Dordrecht: Springer, Netherlands; 2002.
- [45] Panesar AS, Weaver PM. Optimisation of blended bistable laminates for a morphing flap. *Compos Struct Oct.* 2012;94(10):3092–105.